UNIVERSIDADE DE SÃO PAULO

INSTITUTO DE FÍSICA DE SÃO CARLOS

ILAIÁLI SOUZA LEITE

Potential effects of nanostructured protoporphyrin IX-mediated photodynamic therapy in different types of cancer

São Carlos

2020

ILAIÁLI SOUZA LEITE

Potential effects of nanostructured protoporphyrin IX-mediated photodynamic therapy in different types of cancer

Thesis presented to the Graduate Program in Physics at the Instituto de Física de São Carlos, Universidade de São Paulo to obtain the degree of Doctor of Science.

Concentration area: Applied Physics

Option: Biomolecular Physics

Advisor: Dr[a]. Natalia Mayumi Inada

Original Version

São Carlos

2020

Leite, Ilaiáli Souza
Potential effects of nanostructured protoporphyrin IX-mediated photodynamic therapy in different types of cancer / Ilaiáli Souza Leite; advisor Natalia Mayumi Inada -- São Carlos 2020.
84 p.

Thesis (Doctorate - Graduate Program in Biomolecular Physics) -- Instituto de Física de São Carlos, Universidade de São Paulo - Brasil , 2020.

1. Photodynamic therapy. 2. Protoporphyrin IX. 3. Nanotechnology. I. Mayumi Inada, Natalia, advisor. II. Title.

FOLHA DE APROVAÇÃO

Ilaiáli Souza Leite

Tese apresentada ao Instituto de Física de São Carlos da Universidade de São Paulo para obtenção do título de Doutora em Ciências. Área de Concentração: Física Aplicada - Opção: Física Biomolecular.

Aprovado(a) em: 29/04/2020

Comissão Julgadora

Dr(a). Natalia Mayumi Inada

Instituição: (IFSC/USP)

Dr(a). Ana Rosa Lopes Pereira Ribeiro

Instituição: Universidade do Minho/Portugal

Dr(a). Valtencir Zucolotto

Instituição: (IFSC/USP)

Dr(a). Mauricio da Silva Baptista

Instituição: (IQ/USP)

Dr(a). Maiara Lima Castilho

Instituição:UNIVAP/São José dos Campos

To my parents and sister,

who always support me and made me who I am today.

And to my friends, the family I got to choose,

who gave me strenght and constantly made my days shine.

ACKNOWLEDGEMENTS

First things first: I'd like to thank all the people involved in this proccess. It was long and I'm sorry if I forget anyone, I want to express all my gratitude for everyone who helped me, taught me or was there all this time, and I know there were/are A LOT of people. I want to thank them for all the support and kindness, I'm lucky to have had both of them the whole time.

I wish to thank my mother, for showing me everyday how to be strong, kind, empathic and how to apreciate all the beauty in small places. I'd like to thank my father for all the stories he read to us when we were growing. Stories are dreams, and they taught me life is a great adventure we have to face with courage and humor. I'm grateful for my little sister, the strongest person I know, who constantly teaches me how to be a better person. I'm very proud of you! I'd like to thank my "favorite" people, life wouldn't be the same without you, and not even half as fun! Thank you for all the laughs throughout the years, for the companionship, the love, the amazing memories of bad ideas that sounded good back then, the funny mispellings and saying the wrong thing but being understood anyway, the games and singing along, worst-yet-best way ever created (product of boredom, of course) to pick movies, stargazing, endless conversations, competitions and playlists. Specially for things not changing one bit even after months without being able to get together: when we do, it's like we'd met yesterday. Each one of you have a little piece of me.

I'm eternally grateful for my supervisor, Dr. Natalia Inada, whose light and kindness always guided me. I'm very lucky to end up with the very person who inspired me years back, when I was an undergrad, in a talk about how PDT have incredible results in cancer/infections treatment. I remember thinking "that's what I want to do!", not only because it is an awesome techique, but because Natalia spoke with great passion about research and PDT. Through the years, I've seen her enthusiasm, passion and dedication in everything she does, and in every meeting, she compeled us to want to do more, encouraging us with her expertise and kindness. Thank you for being my scientific mom, friend and supervisor, for all the opportunities and collaborations and the pacience and love teaching us. I'd also like to thank prof. Dr. Cristina Kurachi for the teachings and friendship, I'm sure I wouldn't be here today if I hadn't had you as a professor back in 2008. I'd like to thank prof. Dr. Bagnato and Prof. Dr. Francisco for all the help and collaboration, and funding. I'd like to thank prof. Dr. Vivero-Escoto for the collaboration, for all the meetings, discussions and for having me in his lab for 3 weeks, thank

you for making me feel very welcome and introducing me to your wonderful family! I thank Dr. Juliana Cancino-Bernardi and Gabriela Mayr for the awesome collaboration and support!

Without each one of the incredible friends I met from 2006 on in São Carlos and our dear Sala 5, I also wouldn't be me today. Thank you guys for all the killer games, bbqs, weekends at CEFER, karaoke nights, dinners, RPG sessions, "discos espaciais" (even with that unfortunate substitution – tomato IS NOT supposed to be used like that), laughs inside and outside the lab, parties, the amazing friendship, conference travels, Christmas, birthdays, surprise parties and you not giving up on me, not even when I deserved it (print stuff in pro-aluno was indeed a lame excuse). You are awesome and I miss you a lot. A special thanks for everyone in the USP São Carlos Choir, it is a special group of people that cheered me up every Thursday for years. I miss you and I wish you keep making people happy with your lovely tunes. I also want to thank Madrigal Revivis from USP Ribeirão Preto, our Mondays together were amazing, and all the tiredness was woth it, 2018 was a great year because of you! I'd like to thank each member of 5ªD and for all the amazing time we had together last year. We all had to face an intense, diferente and tottaly new environmet, and sharing this experience with you made it unique and special. Thank you for all the laughs, games, lunches, dinners and for being a family when I needed one. Thank you CSI Limeira for the extended 5ªD moments and for starting together this whole new profession, and thank you EPC Limeira, I miss you guys and I am grateful for starting this new career there: you all taught me a lot and made me feel parto f an fantastic team!

I also would like to thank all the Group of Optics members, I miss you and I miss the seminars and the lab. All of you always helped me, with results discussions, sharing protocols and experiences, solving problems and having a great time together! I couldn't forget to thank all my undergrad and grad teachers, thank you for the lessons and teachings in my early years in IFSC. I'd like to thank all the IFSC employees for the kindness and efficiency.

Finally, I'd like to thank CNPq and CEPOF for the funding and financial support.

“Success is the ability to move from one failure

to another without loss of enthusiasm”

-- Sir Winston Churchill

ABSTRACT

LEITE, I. S. **Potential effects of nanostructured protoporphyrin IX-mediated photodynamic therapy in different types of cancer**. 2020. 84 p. Thesis (Doctor in Science) – Instituto de Física de São Carlos, Universidade de São Paulo, São Carlos, 2020.

Light-photoactive substances interactions assessment to promote cell death as therapeutic outcome was initially introduced by Oscar Raab in the late 1800s. Since then, the forementioned technique - photodynamic therapy (PDT) - has been evaluated to treat a wide range of diseases. Cancer, a collection of related diseases, is among the leading causes of mortality worldwide and has been widely evaluated in research and clinical trials using PDT over the past 35 years. Although it may be prescribed for precancerous lesions treatment and some specific types of cancer, its effectiveness is limited by the ineffective photosensitizer buildup at the treatment site. Nanotechnology has addressed the problem of drug delivery through the development of different nanostructured platforms capable of increasing several pharmacological properties of molecules, such as their solubility and their circulating half-life. The association of nanotechnology's potential to improve photosensitizer delivery to target tissues with the oxidative damage of PDT to induce cell death has emerged as a promising prospect for optimizing cancer treatment. In this study, we propose to evaluate the potential of redox-responsive silica nanoparticles and membrane fusogenic liposomes (MFLs) carrying protoporphyrin IX (PpIX) as the selected photosensitizer for melanoma, non-melanoma and breast cancer treatment using PDT *in vitro*. Studies evaluating the impact of different solvents on the free and nanostructured PpIX photostability, the nanoparticles and MFLs internalization, phototoxicity and reactive oxygen species (ROS) were carried out, showing that, despite the aggregation, the molecules and nanoparticles are internalized in sufficient quantity to promote massive damage to cell viability when irradiated with 630 nm.

Keywords: Photodynamic therapy. Protoporphyrin IX. Nanotechnology.

RESUMO

LEITE, I. S. **Potencial efeito de terapia fotodinâmica mediada por protoporfirina IX nanoestruturada em diferentes tipos de câncer**. 2020. 84 p. Tese (Doutorado em Ciências) – Instituto de Física de São Carlos, Universidade de São Paulo, São Carlos, 2020.

A investigação da interação da luz com substâncias fotoativas para promover morte celular foi inicialmente introduzida por Oscar Raab no final dos anos 1800. Desde então, esta técnica – terapia fotodinâmica (TFD) - foi proposta para tratar diversas doenças. O câncer, nome dado a uma coleção de doenças relacionadas entre si, está entre as principais causas de mortalidade no mundo e tem sido amplamente avaliado em pesquisas e ensaios clínicos utilizando TFD nos últimos 35 anos. Embora possa ser prescrita para tratamento de lesões pré-cancerosas e alguns tipos de câncer, sua eficácia é limitada pelo acúmulo ineficaz do fotossensibilizador no local do tratamento. A nanotecnologia tem abordado o problema de entrega de fármacos através do desenvolvimento de distintas plataformas nanoestruturadas capazes de aumentar diversas propriedades farmacológicas de moléculas, como sua solubilidade e sua meia-vida circulante. A associação do potencial da nanotecnologia para melhorar a entrega do fotossensibilizador para os tecidos alvo com o dano oxidativo da TFD para induzir a morte celular tem despontado como perspectiva promissora de otimização do tratamento do câncer. Nesse estudo, foi proposto avaliar o potencial de nanopartículas redox-responsivas de sílica e lipossomas fundíveis com a membrana celular (*menbrane fusogenic liposomes*, MFLs) carreando protoporfirina IX (PpIX) para o tratamento de diferentes tipos de câncer. Estudos avaliando o impacto de diferentes solventes sobre a fotoestabilidade da PpIX livre e nanoestruturada, sua internalização e sua fototoxicidade foram realizados, evidenciando que, apesar da agregação, as moléculas e nanopartículas são internalizadas em quantidade suficiente para promover danos massivos sobre a viabilidade celular quando irradiados com 630 nm. Estudos avaliando a produção de espécies reativas de oxigênio revelaram que, apesar da agregação da PpIX livre, as moléculas e as nanoestruturas são capazes de produzir quantidades suficientes dessas espécies no interior das células, sendo responsáveis pelo dano cellular observados em ensaios de fototoxicidade.

Palavras-chave: Terapia fotodinâmica. Protoporfirina IX. Nanotecnologia.

LIST OF FIGURES

LIST OF TABLES

CONTENTS

1 INTRODUCTION

Cancer is the name attributed to a collection of related diseases, which is among the leading causes of mortality worldwide: in 2018, it was estimated that approximately 9.6 million deaths occurred as a result of these diseases, with statistics indicating that, worldwide, 1 in 6 deaths is due to cancer. Among several types, skin cancer is the most prevalent in the world population, with annual diagnosis of over 1 million new cases. In the female population, breast cancer has the highest prevalence, also affecting men. Regardless of the type of cancer, predictions indicate that over the next 20 years, the incidence and mortality numbers derived from these diseases should increase by 70%. These numbers indicate the necessity to continue investing in developing alternative techniques for cancer treatment.

The interaction between light and photoactive substances, called photosensitizers (PS), to promote cell death was initially investigated by Oscar Raab in the late 1800s. Since then, this technique, called photodynamic therapy (PDT), has been studied to treat a wide range of diseases, and is already clinically approved and indicated for the treatment of some types of cancer. However, its effectiveness is limited by ineffective PS accumulation treatment site. Nanotechnology has addressed the drug delivery problem by developing distinct nanostructured platforms capable of increasing several molecules of interest pharmacological properties, such as solubility and circulating half-life. Intelligent stimulus-responsive systems, releasing the carried molecule more selectively and specifically at the treatment target, have shown promising results in various *in vitro* and preclinical studies. Thus, the association of Nanotechnology to improve FS delivery in targeted tissues with the oxidative damage promoted by PDT to induce cell death has emerged as a promising perspective for cancer treatment optimization.

Thus, the objectives of the present study are to verify and compare the efficiency of 2 nanoplatforms, redox-responsive silica nanoparticles and membrane fusogenic liposomes, carrying protoporphyrin IX in *in vitro* PDT of different tumor cells (derived from: breast cancer, non-melanoma skin cancer and melanoma), to assess its effects on healthy cells and to compare the efficacy of nanocarriers among themselves and with the unmodified PS.

2 LITERATURE REVIEW

2.1 Cancer

Cancer is the generic designation attributed to a collection of related diseases that are characterized by loss of control over the processes of cell differentiation and division.[1] By presenting defects in pathways and regulatory mechanisms that guarantee their normal proliferation and homeostasis, the affected cells begin to proliferate in a disorderly manner and may invade surrounding tissues, occasionally aggressively.[2] These abnormal cells can dettach from their original site and, through the bloodstream or lymphatic system, reach farther tissues, lodge in new sites, where they resume their uncontrolled multiplication, resulting in metastases. The ability to keep their proliferative signaling active, evade growth suppressors, resist mechanisms of cell death, induce angiogenesis, enable their replicative immortality, activate the invasion and metastasis process, evade their recognition and eradication by the immune system, for example, constitute a set of important characteristics identified in tumor cells that enable tumor growth and dissemination.[3]

There are more than 100 different types of cancer, and within the same organ, different subtypes of malignant tumors can be found.[2] Being a complex group of diseases, its cause originates from several factors, from genetic predisposition to external factors such as smoking, alcoholism, prolonged exposure to sunlight, ionizing radiation or some infections caused by viruses, bacteria or parasites.[4-5] Aging also results in a significant increase in the likelihood of developing cancer, as the efficiency of the cellular machinery involved in the process of genetic material replication decreases over time, reducing its accuracy and ability to repair its own errors. Symptoms, as well as treatment, depend on the type of cancer and its stage, and may not be linked to the disease itself but may be a consequence of tumor growth. Diagnosis is usually made initially by imaging techniques such as X-rays, magnetic resonance imaging, ultrasound, endoscopy and tomography, but diagnosis confirmation is achieved by affected tissues biopsy. Early diagnosis greatly increases the chances of treatment effectiveness, which usually involves one or a combination of the following: surgery, radiotherapy and chemotherapy.[6]

According to the International Cancer Research Agency and the World Health Organization, cancer is the second leading cause of mortality worldwide, and in 2012, 2015 and 2018 approximately 8.2, 8.8 and 9.6 million deaths occurred as a result of these diseases, respectively.[6] Cancer incidence has also been increasing over time: in 2008, about 12.7 million new cases were reported, and in 2012 this statistic reached 14.1 million, and estimates indicate

that over the next 20 years, these numbers are likely to increase by 70%.[1-7] In Brazil, it is estimated that 576 thousand new cases were reported in 2014 and approximately 596 thousand in 2016.[8-9]

The skin is the largest organ in the human body and its frequent exposure to a main risk factor, ultraviolet rays from the sun, can cause the development of different types and subtypes of cancer. Each year more than 1 million new cases of skin cancer are diagnosed, and this group of diseases is the most common in the world population.[10] The three main types are: basal cell carcinoma, squamous cell carcinoma (also called epidermoid carcinoma. When refered together with basal cell carcinoma, it is named non-melanoma skin cancer) and cutaneous melanoma. Non-melanoma skin cancer is the most common among skin cancer subtypes and, in the Brazilian population, represents approximately 25% of the malignancies registered in the country. Estimates predict approximately 176,000 new cases of this cancer in 2016 in Brazil.[9] Its mortality rate, however, is the lowest among skin tumors, totaling 1,805 deaths in 2013.[11] Cutaneous melanoma, originated by the cells responsible for melanin production, despite representing a low percentage of malignant skin tumors, is the most aggressive due to its high metastatic capacity.[12] Its worldwide incidence is less than 5% among skin cancer cases, but it is responsible for 95% of deaths caused by this type of cancer.[13] In Brazil, its incidence among skin cancer cases was only 4% in 2013, but the number of deaths caused, 1,559 in total, remained close to non-melanoma skin cancer. The most indicated treatment for melanoma is surgical removal of the tumor, and the indication of radiotherapy / chemotherapy is dependent on the disease stage.[12]

The most common type of cancer in women worldwide, and the second in the Brazilian female population, is breast cancer, representing approximately 25% of new cancer cases reported[14]. It is one of the public health challenges faced by Brazil and several countries, with data revealing that 60% of deaths associated with this cancer occur in emerging countries.[15] This type of cancer is also developed by men, but with low incidence (close to 1%), and in 2013 in Brazil, the total number of deaths attributed to this disease was 14,388, with 181 cases represented by male patients. The National Cancer Institute José Alencar Gomes da Silva (INCA) estimates that in 2016 about 57.960 new cases appeared in the country.[14] Between 1992 and 2012, the number of deaths from breast cancer increased from 6.303 to 13.746.[15] Its treatment varies according to the staging and characteristics of the disease, as well as the patient's conditions, and consists of surgical removal, radiotherapy / chemotherapy.[16]

Regardless of the type of cancer, treatment efficiency and prognosis may be limited to several factors, such as the impossibility of performing surgical removal (due tumor localization or its extension) or the permanence of some cancer cells after surgery. With the high incidence rates and high mortality associated with these diseases, it is necessary to develop new techniques for cancer treatment, or that may be associated with the conventional treatment of these diseases.

2.2 Photodynamic Therapy

Photodynamic therapy (PDT) is a technique which main application has been treating tumors since its first clinical application in 1903, but which is currently being explored to treat different premalignant lesions or pathologies caused by bacteria, viruses and fungi.[17-22] It consists on the interaction of a photoactive substance, called photosensitizer (PS), molecular oxygen at the treatment site and light of specific wavelength, capable of interacting with the photoactive molecules. In its ground state, this molecule has two electrons in a low-energy orbital that have opposite spin orientation (characterizing a singlet state, figure 1). The PS-light interaction promotes the transition of one of these electrons to a higher energy orbital, not modifying its spin. The return to its original state may be due to energy loss through internal conversion to heat, light emission (fluorescence), or the excited singlet state electron may be reversed by a process called intersystem crossing, where the molecule state is then converted to a triplet state (where electrons in the orbital have parallel spins). In this state, the PS can return to its basal state by light emission (phosphorescence) or it can interact with the molecular oxygen in the medium through two reactions, promoting PDT: type 1 - direct interaction PS-substrate with electron transfer, generating radicals that interact with oxygen to produce reactive oxygen species (ROS); type 2 - PS-molecular oxygen interaction, which is originally in the triple state, with energy transfer, producing singlet oxygen. These products are capable of oxidizing cell membranes, organelle membranes, proteins, genetic material and several biomolecules that are found in their viscinities, which may lead to cell death.[23]

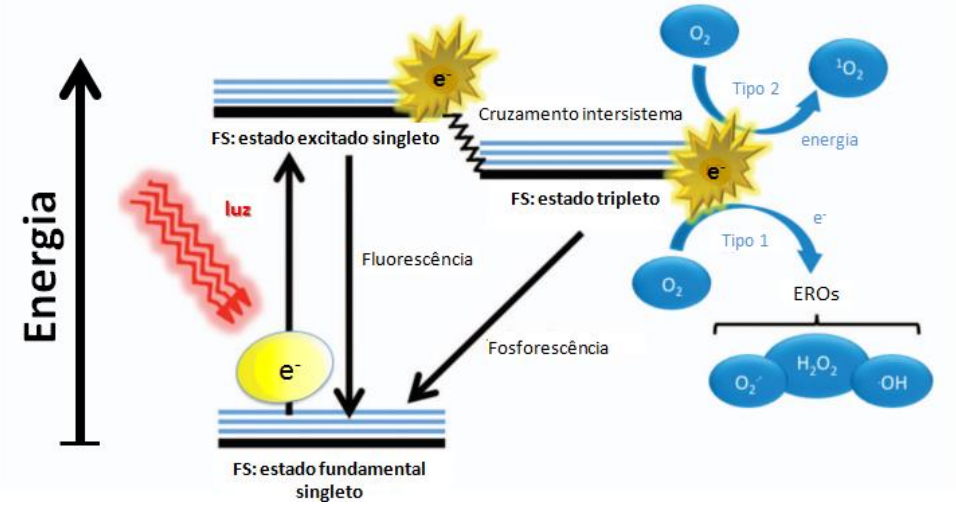

Figure 1 - Schematic illustration of the Jablonski diagram, with the mechanisms involved in PDT. The PS in the singlet ground state is excited and then converted to its triplet state by intersystem crossing. This triplet state can interact with molecular oxygen in two pathways: type 1 (leading to ROS formation) and type 2 (leading to singlet oxygen formation).

Source: Adapted from DENIS *et al*.[24]

PSs are fundamental components in PDT. For clinical applications, characteristics such as low toxicity, selectivity to therapeutic target, ability to be rapidly eliminated by the organism and good quantum yield are limiting factor when selecting the appropriate compound.[25] In oncology, few PSs are currently approved by regulatory agencies around the world: Photofrin® or porfimer sodium (a complex mixture of porphyrins) is used to treat esophageal cancer, non-small cell lung carcinoma and Barret's esophagus); Foscan® or mTHPC (a chlorine) for head and neck squamous cell carcinoma; Levulan®, Metvix® or Metvixia® (aminolevulinic acid - ALA - which is a precursor of the photoactive molecule protoporphyrin IX; or ALA derivatives) for basal cell carcinoma and actinic keratosis (benign neoplasia) treatment.[26-29] However, several clinical studies are ongoing, investigating the potential use of PDT in the clinic for different types of cancer, such as non-melanoma skin that, due to ALA and its derivatives use, has been presenting excellent clinical responses; bile duct, in which the use of Foscan® or Photofrin® has shown good responses to unresectable tumors; pancreas, in which tumor reduction was observed using Verteporfin® (a porphyrin); on female reproductive tract, with high efficacy being verified with methyl ALA application for high grade cervical intraepithelial neoplasms treatment; and brain, investigating Photofrin® use for PDT in recurrent high-grade gliomas.[17,26,28-33]

Clinically, ALA application requires the use of high concentrations of this precursor, since its molecules must first accumulate in the lesion to be incorporated into the heme group

biosynthesis, culminating in the formation of relevant amounts of protoporphyrin IX (PpIX). [34] The major limitation of its use in PDT stems from the low penetration of ALA formulations into the skin, its instability in aqueous pH-neutral solutions, the limited diffusion of the compound through the cell membrane due to its polarity and the heterogeneity in the PpIX formation in tissues, resulting in a restricted PS distribution.[35-36] A possible alternative is the direct use of PpIX, which is an endogenous porphyrin, containing a group of organic heterocyclic dyes with four interconnected pyrrolic rings, which have room, in their center, for one metal ion binding. Its structure, rich in conjugate systems, has intense absorption bands in the visible region of the electromagnetic spectrum, with the peak of the Soret band located near 410 nm and the Q bands (4 in total) at wavelengths between 500 and 700 nm, approximately.[37] Although PpIX has high quantum yield in biological medium and has been extensively studied in PDT, it has dark toxicity and low solubility in aqueous medium, favoring the formation of aggregates that reduce the efficiency of singlet oxygen generation.[36]

The efficacy of PDT is intrinsically linked to the delivery of significant concentrations of PS at the treatment site. Delivery challenges, however, are problems that are not limited to PDT, representing a fundamental problem in the planning and development of drugs. In the specific case of anticancer agents, issues to be considered are the physiological barriers involving the tumor and the tumors own cellular mechanisms, factors that oppose resistance to the accumulation and action of the therapeutic agent at its targeted site, and their distribution, biotransformation and excretion.[38] Characteristics of PSs themselves, such as the hydrophobicity of most of these molecules, which causes their aggregation in aqueous media, also limit the molecules delivery to their destination.[39]

2.3 Nanotechnology

One strategy for optimizing drug and molecules of interest delivery that has been widely used is Nanotechnology. In the last 4-5 decades, this technology has been explored in several areas: energy storage, production and conversion, agriculture, water treatment, disease diagnosis, food processing and storage, construction, electronics, etc.[40] It has multiple definitions, such as the understanding and control of matter in nanoscale dimensions between, in which unique phenomena allow new applications.[41] In the field of Medicine and Pharmacy, its use dates back to the 1960s (figure 2) and the use of various therapeutic products developed with Nanotechnology has since been expanded.[42]

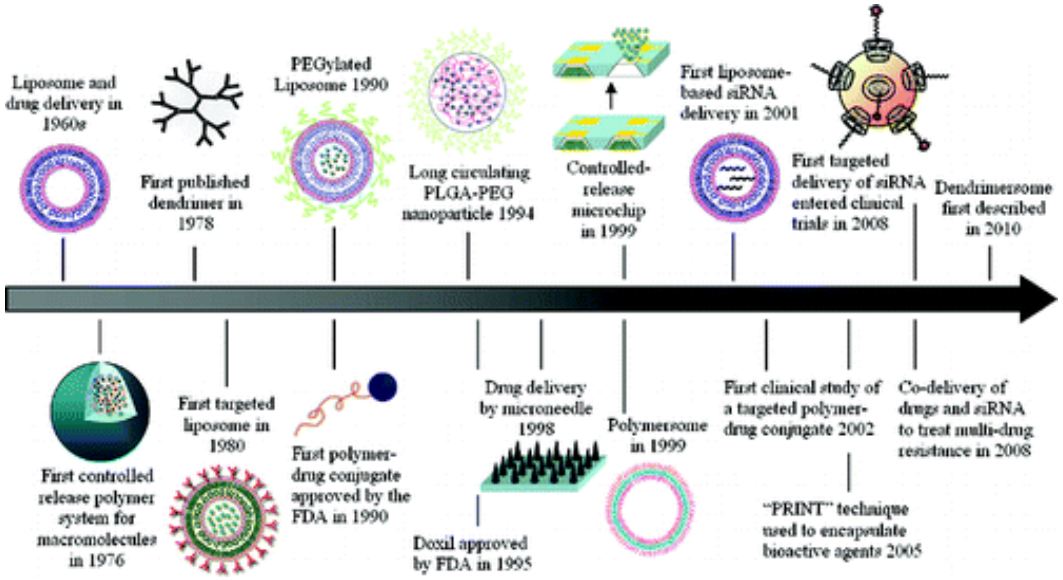

Figure 2 - Chronology of the Nanotechnology-based drug delivery systems development.

Source: CHEN *et al*.[39]

Several nanoscale systems have been developed and are applied in the Biomedical area, such as: nanoparticles, which are colloidal organizations of less than 1 micrometer that may be metallic, polymeric, mesoporous or carbon silica systems; liposomes, which are vesicles in which an aqueous environment is entirely surrounded by one (or more) phospholipid bilayer; micelles, amphiphilic supramolecular structures that are organized to protect hydrophobic molecules within them; dendrimers, radially symmetrical branched structures that are typically characterized by three structural components - a focal center, an inner layer formed by the repetition of its building unit, and the outer layer formed by multiple peripheral functional groups.[38,41,43-46] Specifically for drug delivery systems development, the use of nanocarriers allows therapeutic agents to reach their destination efficiently by increasing their circulation half-life, changing their biodistribution profile, preventing their degradation and excretion by the body.[38,41] Moreover, this preferential and specific accumulation in the therapeutic target promotes toxicity reduction of the compounds employed in the treatments.[42] Strategies such as nanocarrier surface modification allow substances of interest to circulate for a long time throughout the body, since these non-functionalized systems are rapidly opsonized by the mononuclear phagocytic system when present in the bloodstream.[38]

A wide range of nanocarriers have been studied to optimize the delivery of PSs in PDT.[47] Organically modified silica nanoparticles of approximately 20 nm were conjugated to HPPH, a PS belonging to the chlorine class, and tested in colon and fibrosarcoma cancer cells.[48] HMME, a porphyrin, has been conjugated to fullerene nanocomposites with iron oxide nanoparticles

functionalized with polyethylene glycol (PEG) and evaluated in *in vitro* and *in vivo* studies of murine melanoma.[49] PEG-functionalized liposomes carrying m-THPC chlorine showed higher selectivity for induced subcutaneous fibrosarcoma in rats when compared to the commercial form of FS (Foscan®).[50] The use of ALA dendrimers resulted in higher PpIX production in mammary carcinoma cultures when compared to free ALA, and higher PpIX production in macrophages than in endothelial cells, suggesting the possible application of these nanocarriers for breast cancer treatment and atheromatous plaques.[51] Curcuminoid-containing PLGA nanoparticles showed greater stability in aqueous solution when compared to free PSs, photodynamically inactivating *S. aureus* and *C. albicans* in *in vitro* assays.[52]

Despite promising results in *in vivo* studies, the clinical efficiency of nanocarriers is still debated due to the response variability obtained whn assessing the permeability and retention of these systems.[53] This is partly due to the difficulty in controlling the release of the carried molecule at its therapeutic target. One approach that has been explored is the use of stimulus-responsive systems that are able to recognize the microenvironment in which they are inserted and respond to its changes. The stimuli may vary in nature: physical (temperature, electric or magnetic field, for example) or chemical (pH, ions in solution or chemical recognition).[46] Important features of the pathological microenvironment of interest can be used for the design of these intelligent systems, which allows, in principle, the selective and specific delivery of the carried molecules, with their release directly into the therapeutic target. Considering tumors as targets, the oxidative aspect of their extracellular environment and the reducing aspect of the intracellular environment may be explored characteristics when developing redox-responsive systems. These nanostructures are commonly based on the introduction of disulfide bonds that are easily cleaved by glutathione, an antioxidant present in animal cells and found in higher concentrations in tumor cell cytosol when compared to the extracellular environment. Through the imbalance in the levels of this reducing agent, the carried molecules are released in larger quantities inside the tumor cells, increasing the efficiency of drug and other substances delivery.[53-55]

Liposomes are bilayered vesicles that present an internal aqueous cavity completely enclosed by a membrane composed by phospholipids.[57,58] They are considered micro particulate or colloidal carriers that can be prepared with different methodologies, such as biological membranes disruption by sonication, thin-film hydration (where their structural lipids are dissolved in an organic solvent that will be evaporated and the formed films are rehydrated in an aqueous solvent), reverse-phase evaporation, and usually have dimensions

ranging from 50 nm – 5 µm. Due its dual characteristic, liposomes can encapsulate drugs with different solubility, whereas hydrophilic drugs will remain in its aqueous core, and hydrophobic molecules will interact with the phospholipidic bilayer.[57] Liposomes were the first class on nanoparticles to be clinicaly approved for cancer treatment, and it has been showed in several studies that liposomal entraptment improve drug's pharmacokinetics and biodistribution.[59] Liposomes have been widely studied for PDT, with reports of several PS classes successfully being encapsulated and tested over the years.[50-61] It has been reported that liposomes can drastically decrease PS aggragation and change the PS pharmacokinetics due liposomal disintegration on the bloodstream, enhancing treatment efficacy.[59] The first liposomal photosensitizer in clinical practice was Visudyne® (that contains a PpIX derivative, benzoporphyrin derivative monoacid, BPD-MA).[62] Foslip® and Fospeg® are liposomal formulations containing temoporfin that have been extensively evaluated in *in vitro* and pre-clinical studies, showing their efficacy for Gram-positive and Gram-negative bacteria eradication and for oncological PDT.[62] Tipically conventional liposomes are internalized by the cells via endocytosis, with the carried PS remaining on cell organelles, such as lisosomes and mytochondria, but Kim, Santos and Park described the use of membrane fusogenic liposomes (MFLs) to deliver a hydrophobic PS to cell membrane, in order to promote localized cell damage and modulate the type of cell death.[62]

As previously described, the high incidence of cancer, especially breast and skin cancer, creates the demand for alternative or adjunctive treatments to conventional ones. The alliance of optimization of pharmacokinetic properties of substances of interest provided by nanotechnology with the oxidative damage promoted by PDT, a technique that has been showing good results in the treatment of different types of cancer, has resulted in the enhancement of therapeutic activity. Thus, this project proposes to study the association of the two techniques for the treatment of different types of cancer using redox responsive silica nanoparticles carrying PpIX and membrane fusogenic liposomes. The objectives of this work are to compare the results of the use of different nanoparticles, evaluating their specificity and efficacy in neoplastic and healthy cell cultures, to compare their efficiency with that of free PpIX, to study the internalization of nanoparticles and their localization in cells and to evaluate reactive oxygen species generation.

3 OBJECTIVES

The objectives of this work are to evaluate the effects of nanoparticles-mediated PDT mediated on tumor cell lines.

The specific aims are:

- To compare optimal experimental parameter to promote cell death via PDT with different types of nanoparticles: polysilsesquioxane nanoparticles and membrane fusogenic liposomes;

- To compare nanoparticles uptake and PDT outcome to the free PS;

- To compare the distinct nanosystems specificity and efficacy in neoplastic and healthy cell cultures, and to compare their efficiency with free PpIX;

- To evaluate reactive oxygen species generation in cell culture using both nanoparticles systems and free PpIX.

4 REDOX-RESPONSIVE SYSTEM

4.1 Nanoparticles

Through a collaboration established in the first half of 2015 (FAPESP / SPRINT - Process 2015 / 50471-5) with the Prof. Dr. Juan Luis Vivero-Escoto from the Department of Chemistry, University of North Carolina at Charlotte, and his student, Zachary Lyles, redox-responsive polysilsesquioxane nanoparticles (PSilQ) were obtained. PSilQs are crosslinked polymers of silsesquioxanes, an organosilicon compound of formula $[RSiO_{3/2}]n$, which are colorless. Through Si-O-Si bonds, they form a three-dimensional network with several possible organic substituents. The substituent of the studied nanoparticles was PpIX, and different elements were introduced into the synthesis in order to obtain four samples to be evaluated:

i) PSilQ with PpIX nanoparticles, called Ctrl-PpIX-PSilQs (Figure 3A);

ii) PSilQ nanoparticles with the introduction of a disulfide bond mediating the attachment of polymers to PpIX, producing a redox-responsive system called RR-PpIX-PSilQ (Figure 3B);

iii) polyethylene glycol-functionalized redox-responsive PSilQ and PpIX nanoparticles (PEG, a polymer that reduces the formation of corona proteins, also decreasing the recognition and phagocytosis of nanoparticles by immune system cells, increasing their circulation time in the bloodstream); called PEG-RR-PpIX-PSilQs;

iv) PEG and folic acid functionalized redox-responsive PSilQ and PpIX nanoparticles (due the overexpression of folate receptors on the surface of tumor cells), called FA-PEG-RR-PpIX-PSilQs.

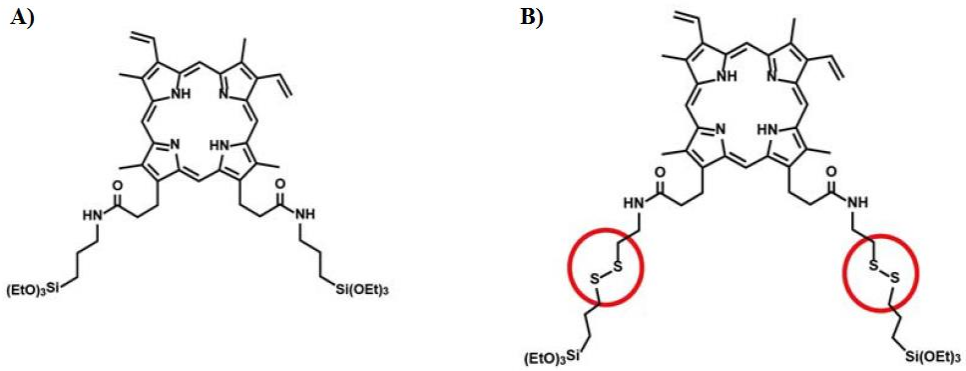

Figure 3 - Chemical structure's schematic representation of A) control (Ctrl-PpIX-PSilQ) and B) redox-responsive (RR-PpIX-PSilQ) nanoparticles of polysilsesquioxane.

Source: Adapted from VIVERO-ESCOTO *et al.*[56]

4.2 Material and Methods

4.2.1 Reagents

Dimethyl sulfoxide (DMSO, Catalog No. D8418) and the NaCl, KCl, Na_2HPO_4 and KH_2PO_4 salts used in the preparation of phosphate saline buffer (PBS) were purchased from Synth (Diadema, SP, Brazil). 3- [4,5-Dimethyl-thiazol-2-yl] -2,5-diphenyltetrazolium bromide (thiazolyl blue tetrazolium bromide, or "MTT" - catalog number M5655), gluthatione (catalog number PHR1359) and protoporphyrin IX (catalog number P8293) were purchased from Sigma-Aldrich (St. Louis, MO, USA). Human mammary adenocarcinoma-derived cell lines (MCF-7, catalog number HTB-22), murine melanoma (B16-F10, CRL-6475) and human squamous cell carcinoma (A-431, CRL-1555) were purchased from the American Type Culture Collection (Manassas, VA, USA); human neonatal dermal fibroblast (HDFn, code C0045C) from Thermo Fischer Scientific (Waltham, NY, USA) and human keratinocytew (HaCaT, catalog number 0341) from the Rio de Janeiro Cell Bank (Rio de Janeiro, RJ, Brazil). DMEM and RPMI 1640 culture media with and without red phenol (DMEM: catalog number. 460 and 574, respectively, RPMI: Catalog No. 462 and 465), as well as the antibiotic penicillin / streptomycin (catalog number 73) and fetal bovine serum (FBS, catalog number 63) were purchased from Cultilab (Campinas, SP, Brazil). ROS probe H2DCFDA (catalog number D399) was acquired from Thermo Fischer Scientific.

4.2.2 Light Source

For sample irradiation, an equipment named Biotable, built by the Technological Support Laboratory of the São Carlos Institute of Physics, was used. The arrangement of 24 LEDs ensures that 24 and 96-well plates are homogeneously irradiated by the base of the well-plates, with a final intensity of 30 mW/cm², considering the attenuation promoted by the acrylic plate bottom. For the study, it was used Biotable with emission centered at 630 nm, so that the wavelength overlaps the last Q-band absorption peak of PpIX (Figure 4). The chosen emission also ensures that light penetration into biological tissue is deeper due to the use of a longer wavelength that remains within the biological optical window while avoiding light absorption by water, melanin and hemoglobin.[63]

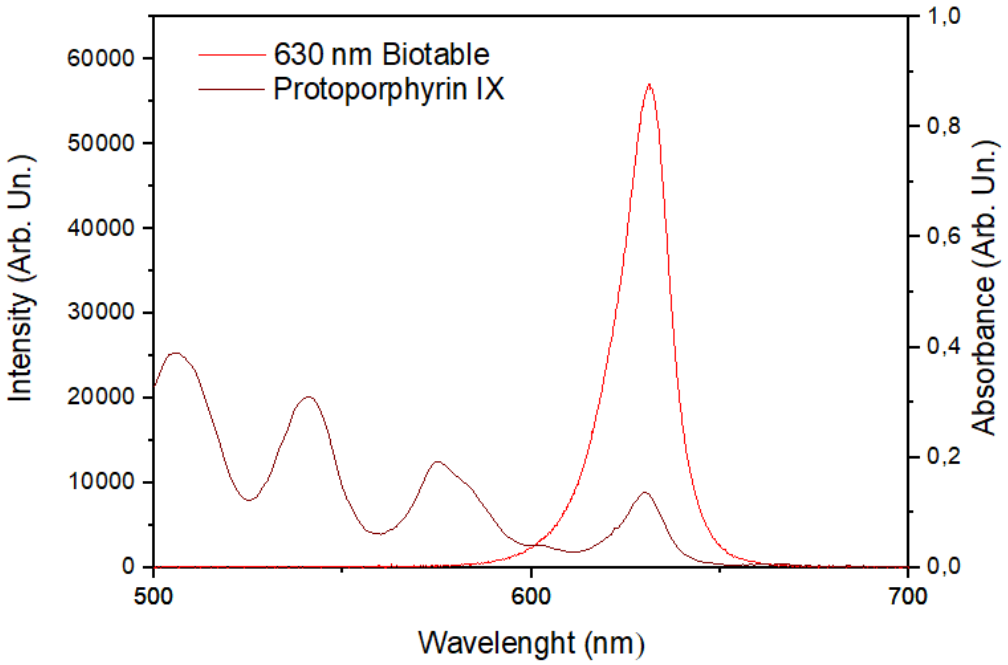

Figure 4 - Emission spectrum of the 630 nm Biotable LEDs (red line) and the PpIX absorbance spectrum in DMSO (brown line).

Source: By the author.

4. 3 Different Solvents Effects on PpIX Photostability

In order to evaluate the influence of solvents on nanoparticles and free PpIX, studies using Fluorescence-lifetime Imaging Microscopy (FLIM) were performed. To this end, the nanoparticles were washed twice, centrifuged at 13.500 rpm for 20 minutes, and resuspended in ethanol (for stock solution stability), in PBS or phenol red-free DMEM supplemented with 1% FBS (free PpIX and RR-PpIX-PSilQ). Free PpIX, which stock solution is made in DMSO to prevent aggregation, was evaluated in the same solvents as nanoparticles. FLIM measurements were acquired by Prof. Dr. Francisco Eduardo Gontijo Guimarães at the São Carlos Institute of Physics Multi-User Laboratory under the LSM 780 inverted fluorescence confocal microscope (Zeiss, Oberkochen, BW, Germany) coupled to the FLIM system (PicoQuant, Berlin, Germany). Sample excitation was performed at 405 nm by a 40 MHz frequency pulsed diode LASER and fluorescence acquisition was performed by the Time-correlated single photon counting (TCSPC) method with SymPhoTime software (PicoQuant, Berlin, Germany). [64]

4. 4 PpIX release and RR-PpIX-PSilQs and Free PpIX Uptake

To confirm the redox-responsive release of PpIX, samples of RR-PpIX-PSilQ were dispersed in DMSO and incubated with 10 mM GSH in quartz cuvette. Initilially fluorescence intensity mesurements were performed in a 5 minute-timelapse, which was gradually increased to 1 hour in order to collect data for 50 hours. The specific time intervals, the fluorescence intensity of the solutions were measured with the Cary Eclipse Fluorescence Spectrophotometer (Agilet, California, USA) using 405/630 as excitation/emission wavelengths. The cuvette remained inside the equipement during the data collection, protected from light, in 37 ºC and constant agitation.

To determine the nanoparticles and free PpIX uptake, studies were performed with laser scanning confocal microscopy LSCM), fluorimetry and flow cytometry. Cells were seeded in CELLview^{TM} cell culture plates (Greiner Bio One, Kremsmünster, Austria) and in 6 and 24-well plates at a density of 10^6 (single and 6-well plates) and 10^5 cells/mL in RPMI 1640 supplemented with 5 % FBS for analysis on inverted LSM 780 confocal microscope, SpectraMax M3 multimodal microplate reader (Molecular Devices, Sunnyvale, CA, USA) and

Accuri C6 Plus flow cytometer (Becton Dickinson, Franklin Lakes, NJ, USA), respectively. After 24 hours, the nanoparticles were washed and resuspended in phenol red-free RPMI supplemented with 1% FBS at a concentration of 75 µg/mL, and the free PpIX solution was prepared in the same medium with the corresponding PpIX concentration found in nanoparticles solutions (15 µg/mL). The samples were incubated for 24 hours at 37ºC and 5% CO_2 atmosphere in a humidified incubator.

For LSCM analyses, cells were carefully washed with PBS twice and images were acquired using a LASER diode emitting 405 nm. For fluorimetric evaluation, cells were washed twice with PBS and lysed with 500 µl of DMSO, incubated for 10 minutes at room temperature. The fluorescence emission of the lysates was then measured on the spectrophotometer, with excitation performed at 407 nm. In flow cytometry analysis, cells were dissociated from the multiwell plates, washed twice, resuspended in PBS and filtered on a 50 µm filter to reduce lumps, and their fluorescence was evaluated on the FL-3 channel (488 nm excitation and 670/LP filter detection) and compared to the fluorescence of the control group (cells that weren't exposed to PpIX/nanoparticles). Experiments on the confocal microscope and flow cytometer were repeated on 2 different occasions, and with melanoma and breast cancer selected as models for tumor cells and fibroblasts as healthy cell model, and fluorescence measurements were performed in quintuplicate of each group and repeated 3 times, performed for breast cancer cells alone.

4.5 *In vitro* PDT Assays

Preliminary tests were performed to determine the light fluence that did not promote cell damage and was able to interact with PpIX, causing cell death via oxidative stress. The MCF-7 breast tumor cell line was exposed in the presence of 75 µg/mL of the Ctrl, RR and PEG-RR-PpIX-PSilQ nanoparticles, a concentration that exhibited good results in Dr. Vivero-Escoto's previous studies of with a similar nanostructured system.[56]

Briefly, two 96-well plates were prepared 24 hours prior to the experiments, seeding 10^5 cells/mL in RPMI 1640 supplemented with 5% SFB and kept in a humidified incubator (MCO-17AC, Sanyo Electric Co. Ltd, Osaka, Japan). After this period, the nanoparticles were washed twice and resuspended in the phenol red-free culture medium supplemented with 1% FBS. The plates were incubated for additional 24 hours in an incubator to ensure nanoparticles

internalization, then washed twice with PBS to remove remaining free nanoparticles in the well supernatant and maintained in 10% FBS phenol red-free medium. One plate was irradiated with the 630 nm Biotable while the other plate remained protected from light exposure during the irradiation. Both plates remained for additional 24 hours in a humidified incubator at 37ºC and 5% CO_2 atmosphere.

Cell viability was determined indirectly by colorimetric assay using MTT, which assesses mitochondrial metabolism (which is commonly associated in the literature as an indirect measure of the percentage of viable cells in samples). The sample supernatant was replaced by phenol-free medium supplemented with only 10% MTT (stock solution: 5 mg/mL) and the plates were incubated again in the oven for 3 hours. All liquid was removed and formazan violet crystals were solubilized with DMSO. Absorbance readings from each well were performed with the Multiskan GO microplate reader (Thermo Fischer Scientific, Waltham, MA, USA) at two wavelengths, as indicated by the reagent manufacturer MTT(64): 570 nm and 690 nm. The viability calculation was performed by subtracting the absorbance value of 570 nm from the resultant reading at 690 nm, and considering the absorbance of the non-irradiated control group as 100% viability. Table 1 shows the summary of the conditions studied in the trials, with each group containing triplicates.

Table 1 - Summary of the experimental conditions assessed in trial using MCF-7 cells.

Groups	Concentration (µg/mL)	Incubation time (h)	Fluence (J/cm²)
Control	-	24	1
Ctrl-PpIX-PSilQ	75		5
RR-PpIX-PSilQ			25
PEG-RR- PpIX-PSilQ			40
			50

Source: By the author.

After assessing the optimal light fluence for PDT experiments (50 J/cm²), 3 repetitions were performed with the MCF-7 cell line (n = 9) including nanoparticles containing folic acid in the study. To compare the nanoparticles effectiveness with the free FS's, cells were exposed to 15 µg / mL PpIX solutions (which corresponds to PpIX's concentration in nanoparticles solutions) and a DMSO control group (which was introduced as a control due the preparation

of PpIX stock solution in this solvent). The same experimental protocol was repeated with A-431 and HaCaT cell lines, to evaluate the effect of PpIX nanoparticles-mediated PDT on different types of cancer and on an important healthy cell for skin studies, respectivelly. To evaluate the response of a tumor and a healthy cell line to different concentrations of PpIX-PSilQ nanoparticles, the previously described experimental protocol (fixing the incubation time and light fluence at 24 hours and 50 J/cm²) was conducted with murine melanoma cell line (B16-F10) and dermal fibroblasts (HDFn). In this study, a wide concentration range of PpIX-PSilQ nanoparticles solutions (50 - 300 μg/mL) was evaluated.

4.6 Reactive Oxygen Species (ROS) Quantification

In order to verify if cell damage was promoted by PDT activity, the ROS production was assessed in *in* vitro experiments emulating PDT assays. Experiments were performed as described in session 3.2.5, introducing the cell permeant probe H2DCFDA, which becomes fluorescent in the presence of ROS after cleavage by intracellular esterases. Briefly, 10^5 cells/mL were seeded in 96 well plates in phenol red-free medium supplemented with 1 % FBS, and incubated with 75 μg/mL of RR-PpIX-PSilQ solution or 15 μg/mL of free PpIX for 24 hours in a humidified incubator. Cells were exposed to the ROS probe 30 minutes before the irradiation, by carefully washing the samples twice with PBS and introducing a fresh 10 μM H2DCFDA working solution, prepared in PBS immedially before its use, in the well plates. Samples were washed twice with PBS and phenol-free medium was added to the cells before exposure to 50 J/cm² (dark control groups remained protected from light). ROS production was quantifyied by H2DCFDA fluorescence intensity readings using 485 nm as excitation, measuring 520 nm emission with the multimodal microplate reader SpectraMax M3 (Molecular Devices, Sunnyvale, CA, USA). Breats cancer cells were selected to compare RR-PpIX-PSilQ and free PpIX ROS production in the presence and absence of 630 nm, and melanoma cells and fibroblast to compare differences in tumor and healthy cell RR-PpIX-PSilQ-mediated PDT.

4.7 Statistical Analysis

Cell viability data was expressed as the mean ± standard deviation of the groups. Statistical analysis was performed using GraphPad Prism 5 (GRaphPad Software, San Diego, California, USA), aplying one-way ANOVA followed by Tukey's multiple comparison test. Each group was performed in triplicates and repeated in three different occasions, resulting in n = 9. Normality evaluation of samples occasionally did not present a normal distribution, so One-Way ANOVA application was performed outside the assumptions provided by this test. Differences between groups were considered statiscally significant when comparisons showed a value of $p \leq 0.05$, indicated in the graph by *.

4.8 Results and Discussion

4.8.1 PpIX Photostability

Important information about the interaction between the fluorophores of interest and the molecular environment in which they are immersed can be extracted from the fluorescence decay time. In particular, it is possible to evaluate molecules aggregation due fluorescence decay times alterations, since non-radioactive decays of the excited states are significant in aggregates, due to the energy transfer between very close molecules.[65] In order to observe the photostability of free and nanostructured PpIX, experiments evaluating the molecules and nanoparticles fluorescence lifetime in different solvents were carried out. From FLIM images, the fluorescence decay times were measured (in figure 5) and exposed in table 2. For decays ruled by two exponentials behaviors, values of the fast decay time (the one presenting the highest slope in the figure) were called τ_1, and the slow (lowest slope) were called τ_2.

Figure 5 shows that, when samples are dispersed in alcohol, fluorescence lifetime is longer than when PBS is used as a solvent. Free PpIX presented, among all the evaluated samples, the longest decay time when solubilized in ethanol, revealing a monoexponential decay of the fluorescence lifetime, which results in the absence τ_1. This suggests that the energy transfer between PpIX molecules is non-existent or very low, indicating the almost exclusive presence of the PS monomeric form in ethanol (which is also evidenced by the Gaussian

distribution seen in the histogram in figure 5D). Changes in the molecular environment introduced by the use of PBS or DMEM with 1% FBS is reflected in the fluorescence decay time, which is reduced from 13.5 ns to 9.7 and 11.62 ns, respectively, resulting in changes on the histogram profile. In addition, it was possible to detect τ_1, requiring the use of 2 exponentials to fit the decay curve. The presence of aggregates is highlighted by the reduction in the PpIX fluorescence lifetime as well as by the emission efficiency reduction, which was observed by comparing fluorescence emission spectra (data not shown).[66]

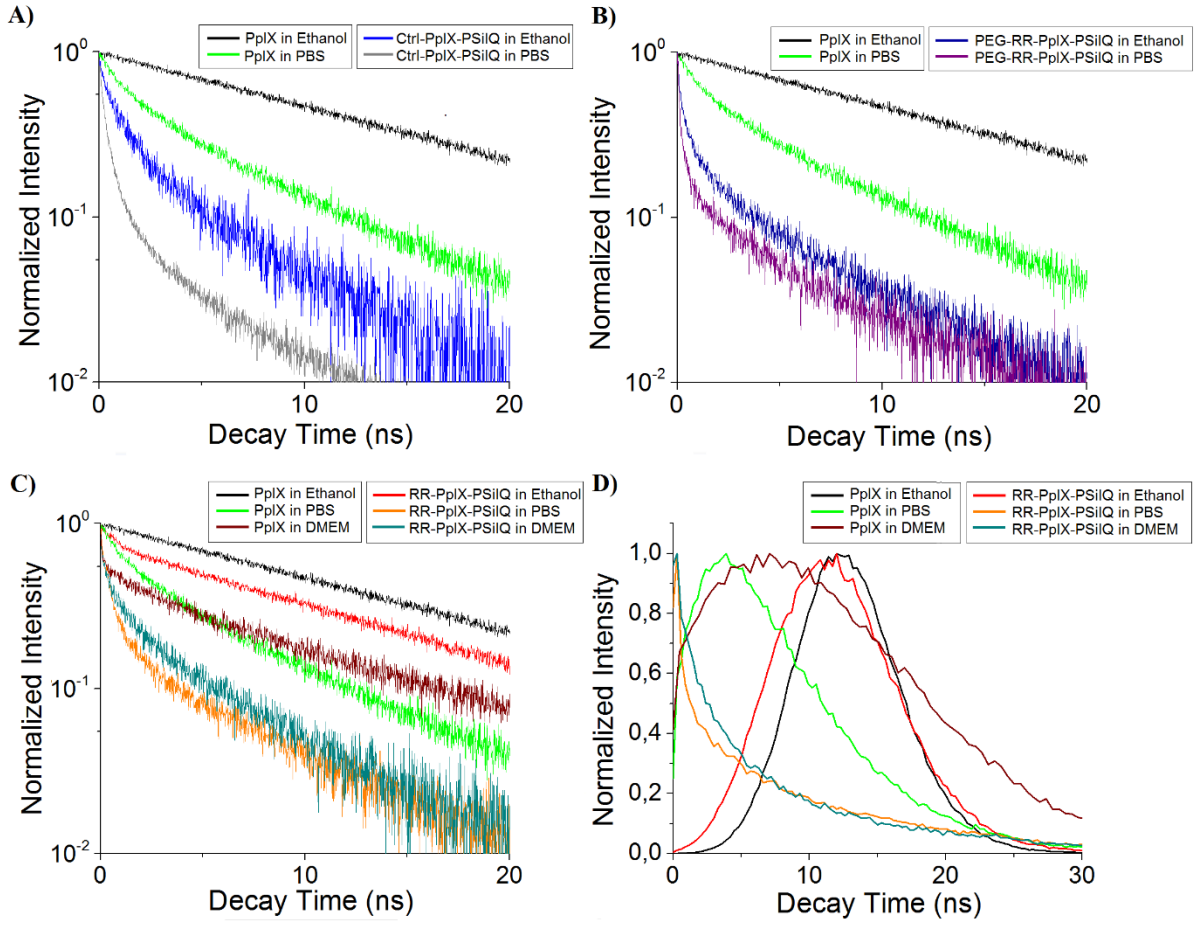

Figure 5 - Fluorescence decay time of free PpIX and the following nanoparticles: A) Ctrl-PpIX-PsilQ, B) PEG-RR-PpIX-PsilQ in ethanol and PBS, and C) RR-PpIX-PsilQ in ethanol, PBS and DMEM with 1% SFB. The decay time histogram of free PpIX and RR-PpIX-PSilQ is shown in D (the other histograms are not displayed due to the similar behavior of the nanoparticles in the different solvents).

Source: By the author

When evaluating the nanoparticles in ethanol, no monoexponential decay is observed and the decay times are shown to be shorter than free PpIX's, suggesting the PS aggregation. This behaviour was already expected due to the tight packaging of PpIX in the nanostructure, which approximates the molecules, allowing their interaction and energy transfer between

them. In particular, Ctrl-PpIX-PSilQ and PEG-RR-PpIX-PSilQ nanoparticles have decay times much shorter than free PpIX, most likely due to the aggregation in media, which is verified by the presence of brown dots in the solutions and the greater difficulty to redispersed these samples even when using a ultrasound bath. This hypothesis is reinforced by the small difference introduced in fluorescence decay times when PBS is used as solvent. The redox-responsive sample, however, shows a strong reduction in this parameter when it is prepared in PBS or culture medium, with promotes a shift in the histogram populations. Both effects reveal the formation of aggregates in the solutions, which potentially results in lower nanoparticle internalization by the cells due to their enhanced dimensions.

Table 2 - Nanoparticles and free PpIX fluorescence decay times in different solvents.

Sample	Ethanol		PBS		DMEM	
	τ_1 (ns)	τ_2 (ns)	τ_1 (ns)	τ_2 (ns)	τ_1 (ns)	τ_2 (ns)
PpIX	-	13,52	1,41	9,67	0,83	11,62
Ctrl-PpIX-PSilQ	0,95	6,28	0,39	5,5	-	-
RR-PpIX-PSilQ	0,94	12,16	0,34	6,67	0,62	6,4
PEG-RR-PpIX-PSilQ	0,41	6,24	0,17	6,22	-	-

Source: By the author.

4.8.2 PpIX release under reducing conditions and Nanostructured vs. Free PpIX Internalization

Before assessing nanoparticles internalization, it was important to determine if the nanosystems were able to properly release the PS in its monomeric form in a reducing environment. For that, experiments were carried out using gluthatione (GSH) in similar concentrations found inside mammalian cells (10 mM) to track PpIX release over time. By measuring the solution fluorescence intensity using 405/630 nm excitation/emission, an increase in this parameter relates to an increase of free PpIX molecules, since the PS is found tightly packed when attached to the nanoparticles, which favors quenching.

During the full extent of the 50 hours, it was observed an increase on fluorescence intensity, which was initiated by GSH addition into the solution (indicated by the arrow in figure 6). This data suggests that free PpIX was continuously released in the solution over time. The lack of a maximum value and signal intensity stagnation suggests that, over the 50 hours, there were still assembled nanoparticles with attached PpIX.

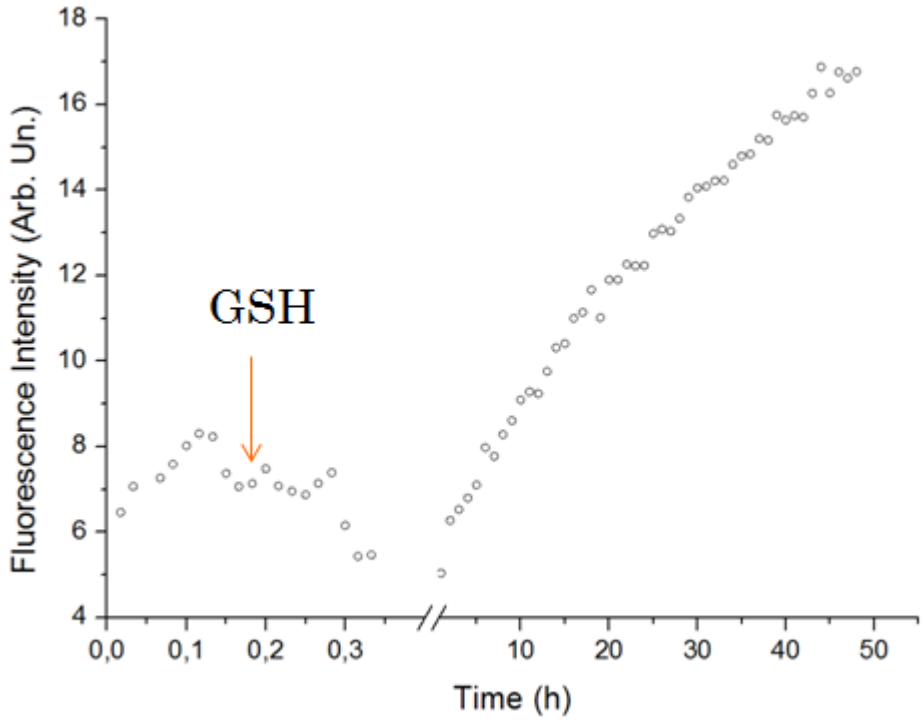

Figure 6 - PpIX release profile after adding 10 mM GSH (the exact time the GSH was added is indicated with an arrow).

Source: By the author.

To determine the nanoparticles internalization by the cells, which allows their degradation by reducing species in the intracellular environment and PpIX release in its monomeric form at treatment target, uptake studies were carried out with different techniques. Breast cancer cells were initially chosen due to the reasonable proportion between their cytoplasm and nucleus, facilitating PS distribution observation in the cytosol. To compare nanoparticle and the PS behavior differences under the same conditions, redox-responsive nanoparticles and the free PpIX were selected for this study.

LSCM images, obtainded after 24 hours of incubation, reveals that free PpIX, despite the presence of visible small aggregates in the solutions, is internalized in large ammounts and

is distributed homogeneously throughout the cytoplasm (figure 7). The same behaviour wasn't observed in samples incubated with redox-responsive nanoparticles, which, after careful sample washing, were observed as aggregates in the supernatant, most likely because they were attached to the glass or to cell membranes. These aggregates were also observed inside the cells, indicating that nanoparticles have been internalized and that they are probably still retained in endosomes or endolysosomes after the evaluated timelapse. This observation is consistent with the main nanoparticles uptake mechanism by mammalian cells, endocytosis.

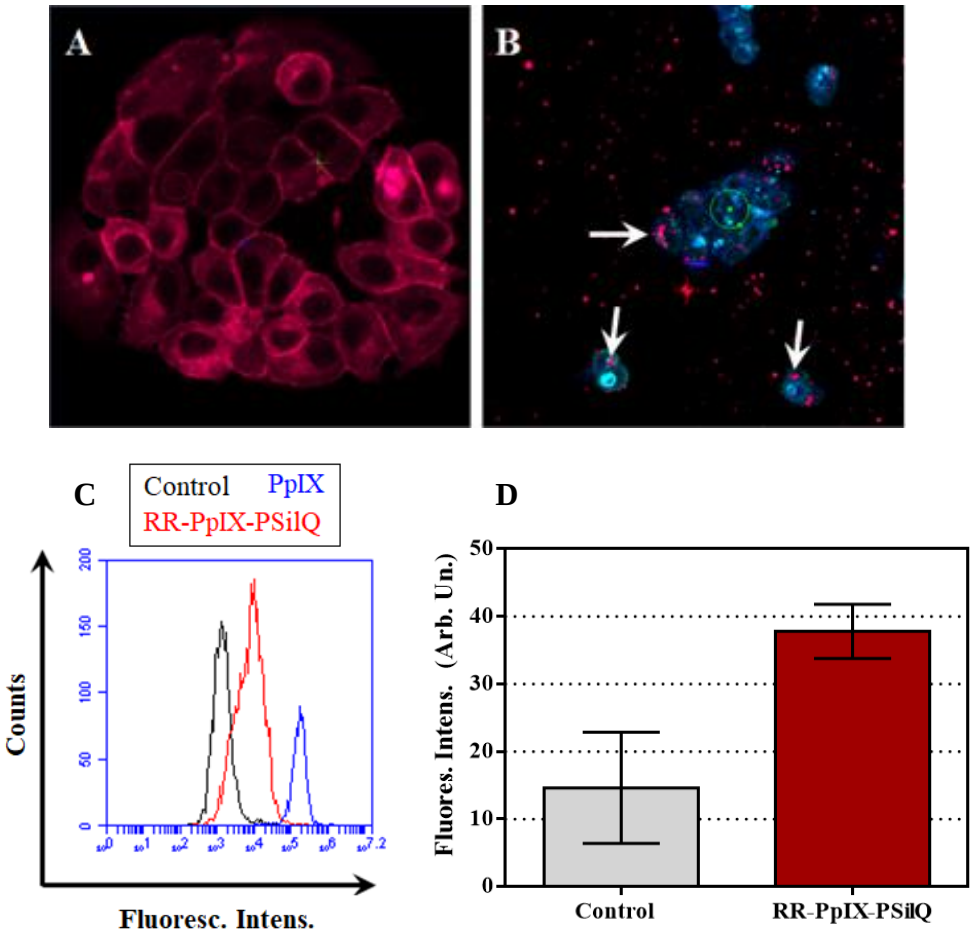

Figure 7 - Assessment of cell uptake by: LSCM of A) free PpIX and B) RR-PpIX-PSilQ (with white arrows indicating aggregates inside the cells), C) flow cytometry using the FL-3 channel and D) measurement of the cell lysates fluorescence intensity of samples incubated with and without RR-PpIX-PSilQ, using 407 nm as excitation and emission as 630 nm.

Souce: By the author.

To confirm the nanoparticle's uptake that was observed by LSCM, cells were subjected to the same experimental protocol (same nanoparticles/free PpIX concentration and incubation

time) for further analysis by flow cytometry. Results show (figure 7C) the cells autofluorescence intensity signal in black, with a displacement of the population that was exposed to the the nanoparticles (red curve in figure 7C) towards higher fluorescence intensity in the FL-3 channel. This indicates that cells in this population present increased fluorescence signal when compared to the control group, suggesting PpIX internalization after their exposur tho the nanoparticles for 24 hours. The population of cells incubated with free PpIX shows a greater displacement (blue curve in figure 7C), which is in accordance with the free PpIX uptake profile verified by LSCM.

Fluorimetry results evaluated the PpIX fluorescence signal (individualized by choosing the proper excitation and emission wavelengths) of cell lysates, allowin the assessment of their cytoplasmatic content. As shown in figure 7D, it is possible to verify an increase in fluorescence intensity of cells exposed to nanoparticles, when compared to the control group. This augmentation in PpIX fluorescence signal corroborates the pervious results suggesting the nanoparticles uptake and availability of PpIX inside the cells after the 24-hour interval.

Nanoparticles selectivity to tumor cells assessment was carried out in uptake studies using melanoma cells (B16-F10) and fibroblasts (HDFn). LSCM images display the increase of fluorescence signal inside the cells for both cell lines when they are exposed to 75 µg/mL of RR-PpIX-PSilQ, but the intense autofluorescence yielded by the healthy cell lines interferes with visual interpretation of nanoparticle internalization (figure 8A). Flow cytometry, however, shows that there is an increase in the fluorescence signal intensity for both cells after nanoparticle incubation. However, it also reveals that the tumor cell line present increased nanoparticle uptake in the evaluated time when compared to the healthy cells due the larger displacement of cell population towards higher fluorescence intensity.

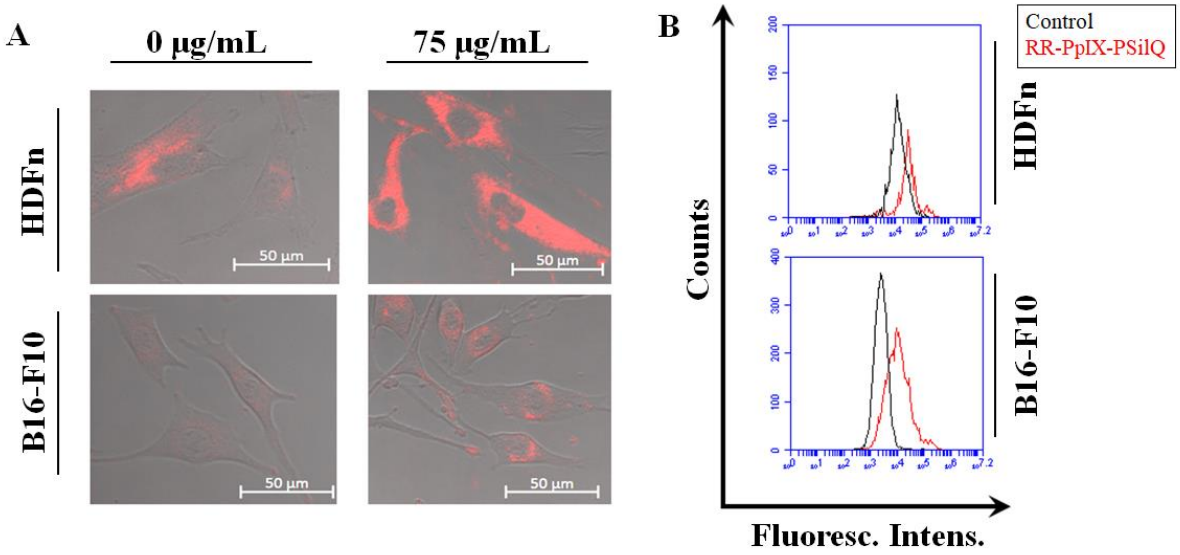

Figure 8 - Assessment of RR-PpIX-PSilQ uptake in healthy (fibroblasts: HDFn) and tumor (melanoma: B16-F10) cells using A) LSCM and B) flow cytometry.

Source: By the author.

4.8.3 PDT: cancer vs. healthy cells

4.8.3.1 Preliminary assessment for optimal light fluence determination

As described in section 2.2, light is one of the three key elements for PDT. The determination of adequate light fluence is essential for treatment efficacy, so that the incident light is able to properly excite the PS in order to produce significant amounts of ROS. Thus, PDT studies started by conducting preliminary tests in which the concentration of nanoparticles and the incubation time evaluated in the uptake experiments remained fixed, with light fluence variations. The summary of the preliminar experiments, describing the experimental condition and the mean value of cell viability is shown in table 3.

Table 3 – Cell viability mean values obtained in preliminary experiments with distinct light fluences (λ = 630 nm).

Cell viability (%)						
	Light Fluence (J/cm²)					
Groups	**0**	**1**	**5**	**25**	**40**	**50**
Control	100±5,7	105,8±2,3	82,2±3,6	90,4±2,8	98,2±5,9	80,8±4,6
Ctrl-PpIX-PSilQ	91,3±2,9	96,2±2,9	69,7±1,3	79,0±3,0	47,2±1,8	31,3±2,8
RR-PpIX-PSilQ	85,7±5,3	93,2±2,9	70,26±3,1	56,4±5,6	24,9±2,5	13,5±7,3
PEG-RR- PpIX-PSilQ	97,8±7,1	86,6±3,3	80,1±4,6	98,9±2,9	90,7±9,1	39,8±0,1

Source: By the author.

It was verified that, in lower light fluences, limited phototoxic effect was produced in the samples, regardless of the nanocarrier that was applied. However, at 40 J/cm², a significant reduction in cell viability mean values was produced. When 50 J/cm² was evaluated, the redox-responsive nanosystem was able to promote death of approximately 87 % of the cells. This ligh fluence, however, had small impact on cell viability by itself, at which point the increase in this parameter could be detrimental to the samples. It is important to point that this parameter is experimentally set through properly controling the time of samples exposure to light: light fluence is determined by the following equation:

$$F = I.t$$

where F stands for light fluence, I is the light source's fluence rate and t is the time of exposure. For a fluency of 50 J/cm², the samples remained 27 minutes and 47 seconds outside the humidified incubator, so higher fluences could promote further stress in the cultures due prolonged time outside the ideal conditions for cell growth. Therefore it was determined to fix light fluence at 50 J/cm².

4.8.3.2 PDT under optimal conditions

After determining the light fluence, PDT experiments with MCF-7 cell line were performed, with the inclusion of a new nanoparticle, functionalized with folic acid, and free PpIX (figure 9).

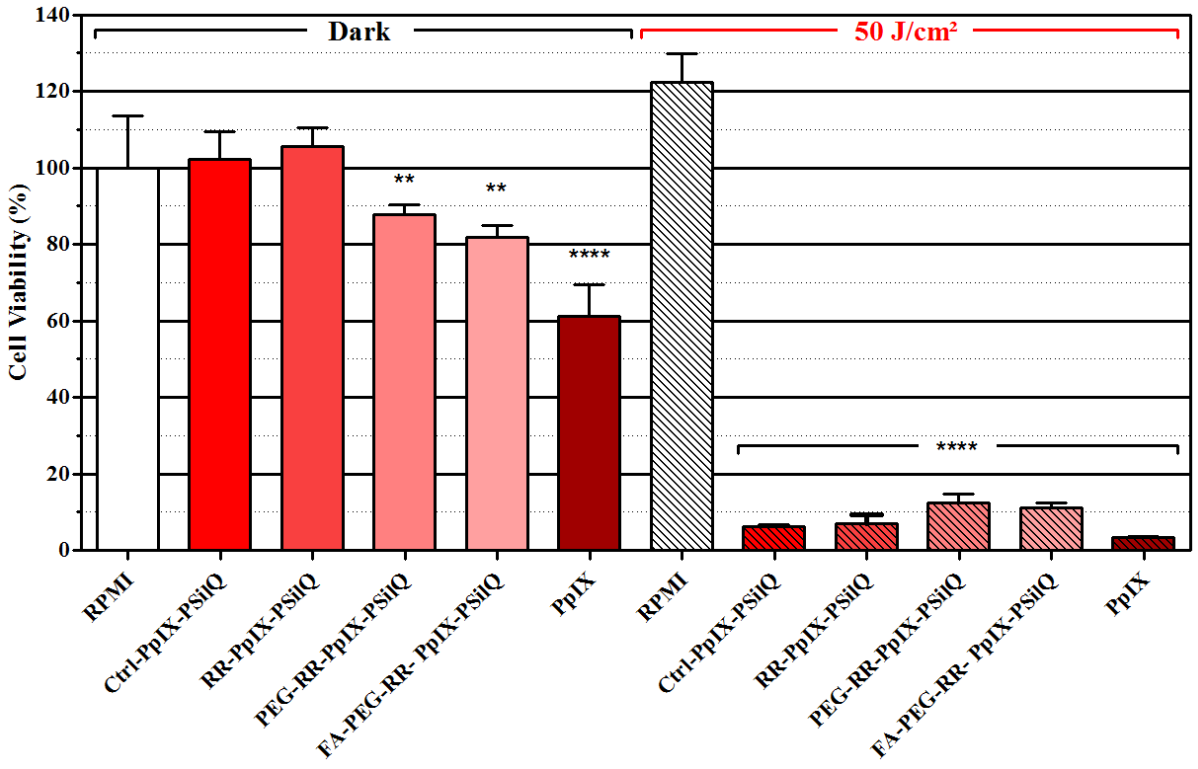

Figure 9 - Free PpIX and nanostructured PpIX-mediated PDT in breast tumor cell cultures (MCF-7). Results are displayed as mean values of cell viability, and ** indicates $p \leq 0.005$ and ****, $p \leq 0.00005$.

Source: By the author.

Groups containing cells that were exposed to nanoparticles but were kept in the dark (nanoparticle dark control groups) displayed reduced or no cytotoxicity, and that the percentage of DMSO that was used to prepare free PpIX solutions does not interfere with the cell viability (DMSO control group). Free PpIX, however, exhibited considerable cytotoxicity by itself, with viability values close to 60 %. After irradiation with 50 J/cm², cell viability of the control group (cells that weren't exposed to nanoparticles nor free PpIX, tagged as "RPMI" in figure 9) remained unchanged, as well as that of the DMSO control. Irradiation of the 4 nanoparticle systems resulted in high phototoxicity, with an average of 7 and 10% of cells remaining viable after exposure to Ctrl-PpIX/RR-PpIX-PsilQ and PEG/AF-PEG-RR-PpIX-PsilQ, respectively.

Cells exposed to free PpIX and light also yielded a significant reduction in their viability value, which remained around 5%. These results show that, although nanoparticles and free PpIX present aggregation in culture medium, as seen in section 4.7.2, the PS inside the cells (in larger quantities when in its free form) is efficiently excited and promote extensive damage to MCF-7 cultures.

To evaluate the effectiveness of the nanoparticles and their potential application in different types of tumors, the same protocol was evaluated in cultures of non-melanoma cancer cells (figure 10). It was observed that this strain is more prone the nanoparticles and free PpIX cytotoxicity (in the absence of light), as the cells viability remained close to 67, 45 and 30% in the Ctrl-PpIX/RR-PpIX-PsilQ, PEG/AF-PEG-RR-PpIX-PsilQ and free PpIX groups, respectively. However, when irradiated, the results became very similar to those obtained with MCF-7 cells.

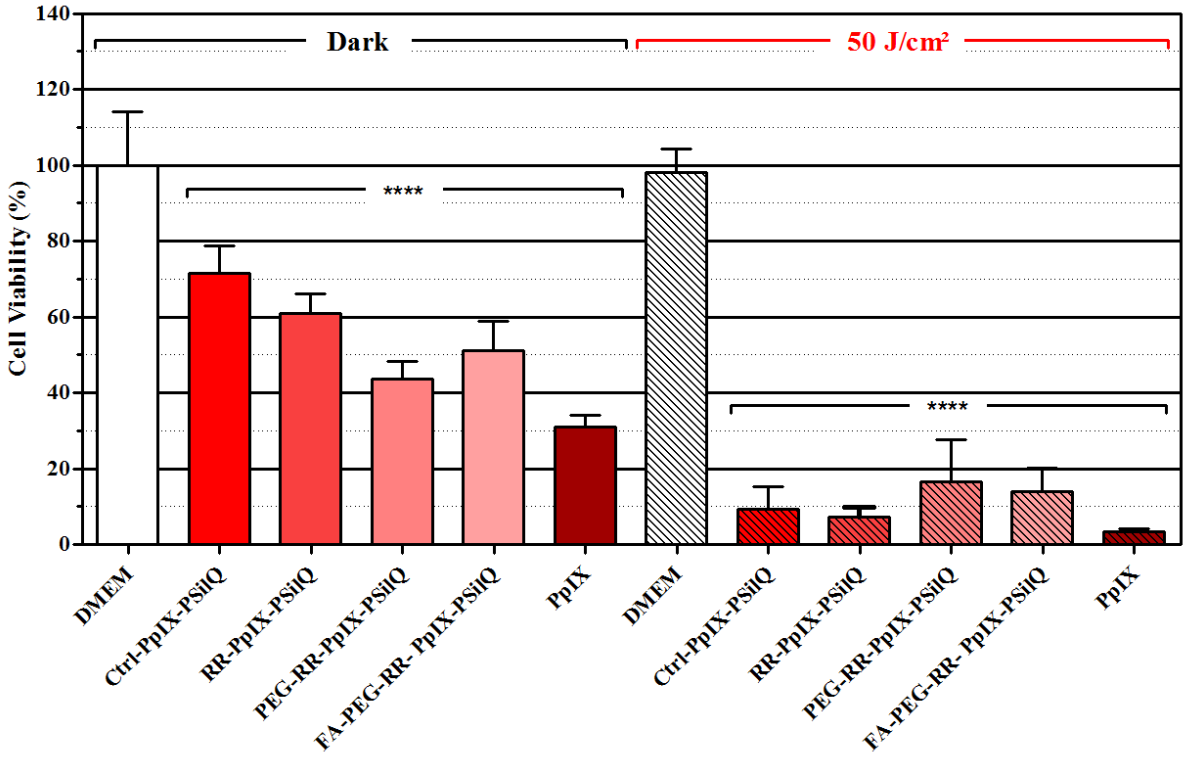

Figure 10 - Free PpIX and nanostructured PpIX-mediated PDT in non-melanoma skin cancer cell cultures (A-431). Results are displayed as mean values of cell viability, and ** indicates $p \leq 0.005$ and ****, $p \leq 0.00005$.

Source: By the author.

To assess whether nanostructured systems have selective behavior (with greater affinity for tumor cells), the outlined protocol was used in cultures of normal skin cells, more

specifically keratinocytes and fibroblasts (HaCaT and HDFn, figure 11 and 12, respectivelly). For keratinocytes, when protected form light exposure, cells were susceptible to the redox-responsive nanoparticles, with viability values remaining between 58 and 73%, with PpIX displaying its elevated cytotoxicity, with aproximately 40% of the cells remaining viable after being exposed to the PS. Cell exposed to nanoparticles and irradiation displayed the same results previously observed for the tumor cell lines, with a slightly increase on cell death mean values: almost 4% of the cells remained viable, which was also observed in the free PpIX group. The only group that presented a diverting behavior from the previous obtained was PEG-RR-PpIX-PSilQ-mediated PDT, yielding cell viability values of approximately 40%. When fibroblasts were submitted to the same experimental protocol, a similar cytotoxicity was observed when applying free PpIX. Cells displayed slightly higher tolerance to the nanoparticles impact on their viability when compared with keratinocytes, with cell viability values fluctuating from approximately 60 to 90 %. PDT groups yielded the previously observed cell death rates.

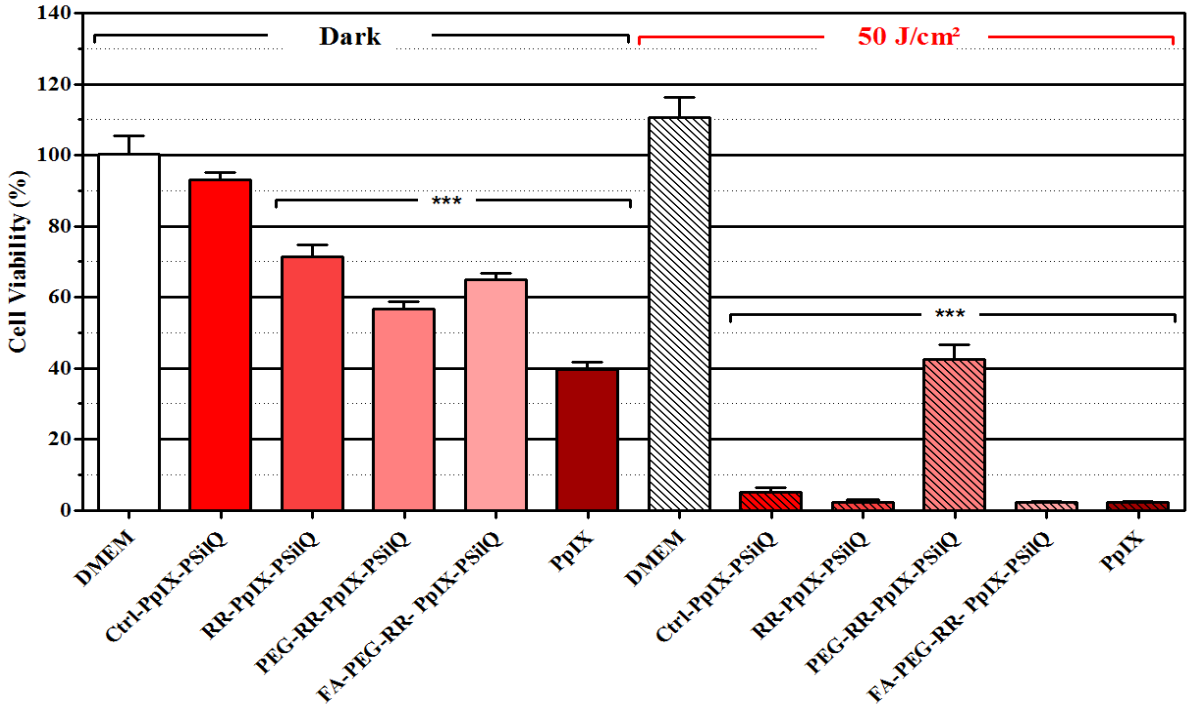

Figure 11 - Free PpIX and nanostructured PpIX-mediated PDT in keratinocytes cultures (HaCaT). Results are displayed as mean values of cell viability, and ** indicates $p \leq 0.005$ and ****, $p \leq 0.00005$.

Source: By the author.

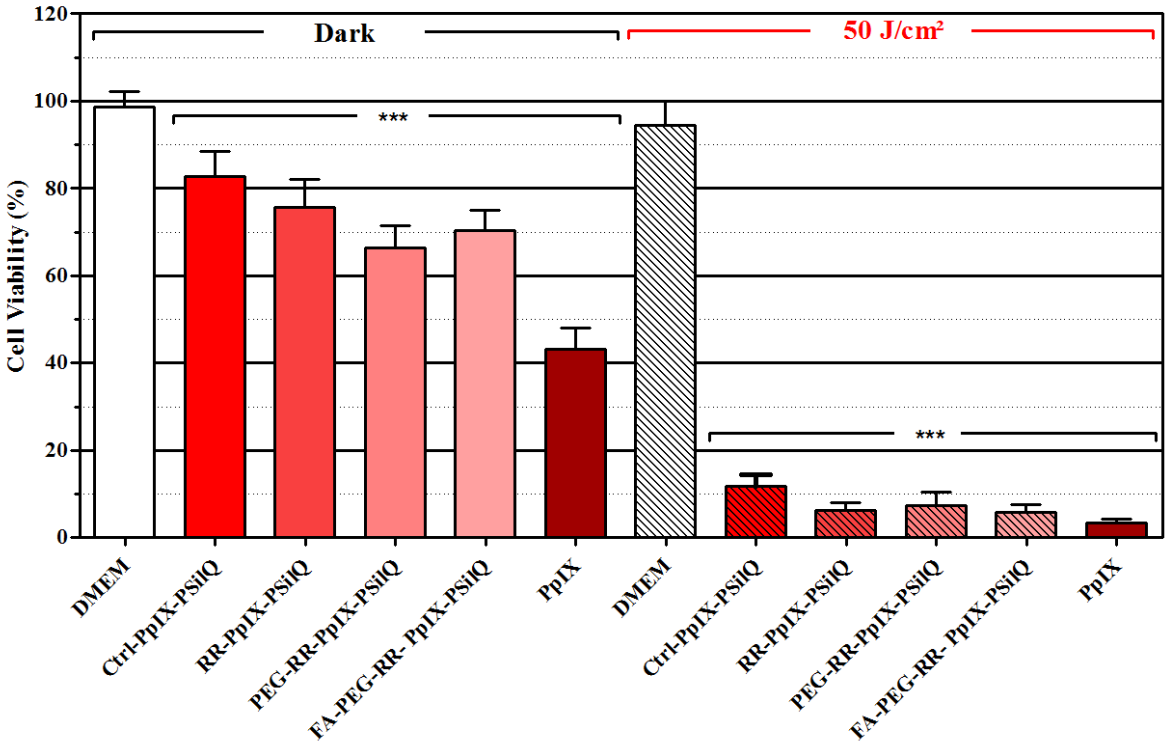

Figure 12 - Free PpIX and nanostructured PpIX-mediated PDT in keratinocytes cultures (HaCaT). Results are displayed as mean values of cell viability, and ** indicates $p \leq 0.005$ and ****, $p \leq 0.00005$.

Source: By the author.

4.8.3.3 PDT: nanoparticles selectivity

So far, light exclusively the impact caused in cell viability through variations in light fluence have been evaluated. The absence of the nanosystem's selectivity in the described cell lines may be due to the use of far too elevated nanoparticles concentrations. Therefore, experiments were performed with Ctrl-PpIX/RR-PpIX/PEG-RR-PpIX-PSilQ, in which the incubation time and light fluence were fixed (24 hours, 50 J/cm²), evaluating distinct nanoparticle concentrations (50 to 300 µg/m, as displayed in figure 13). Evaluation of nanoparticles selectivity was conducted by comparing the same experimental protocol in tumor and healthy cell lines, using melanoma (B16-F10) and fibroblasts (HDFn) as models, respectively.

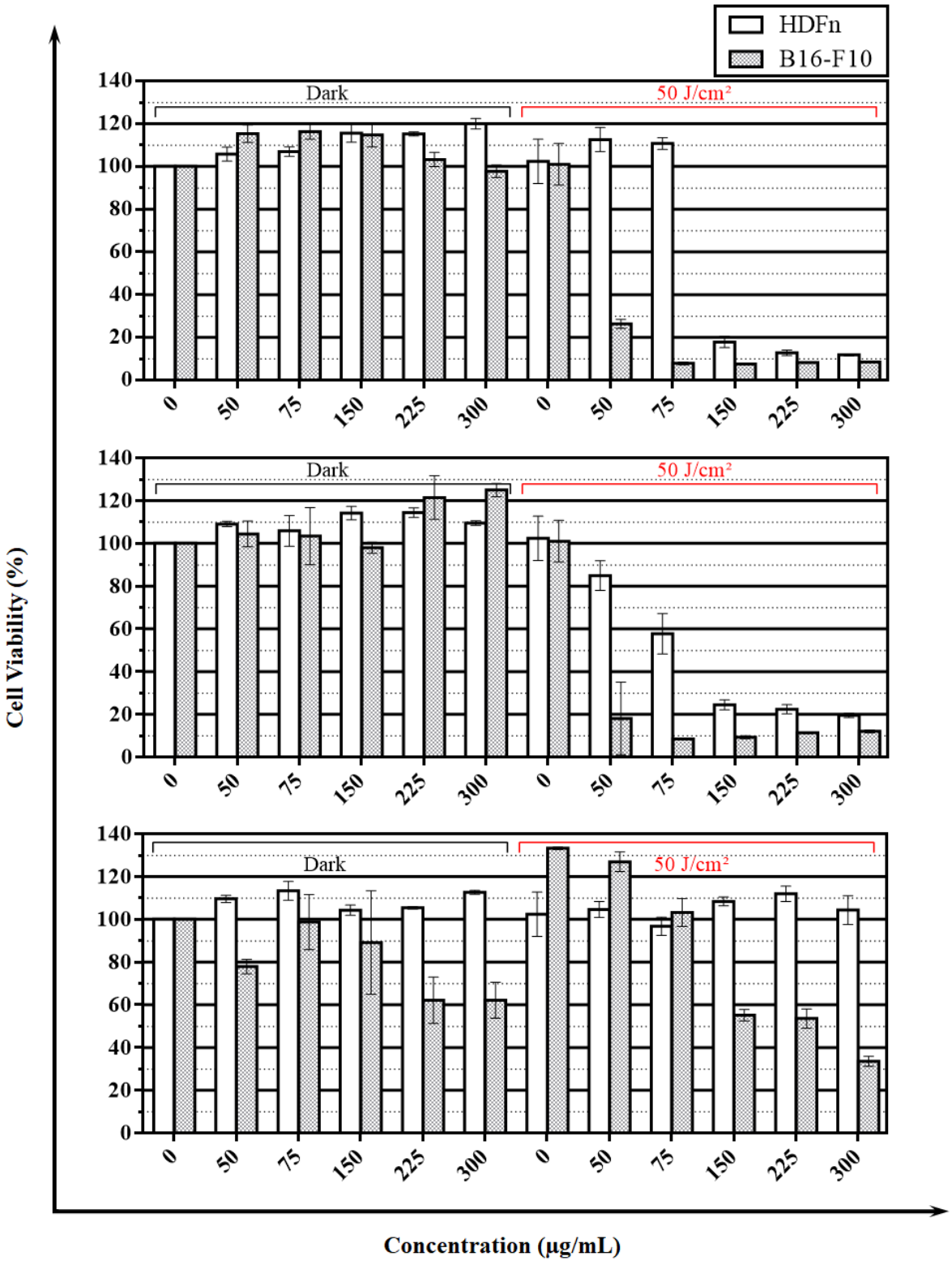

Figure 13 - PDT results when different concentrations of A) Ctrl-PpIX-PSilQ, B) RR-PpIX-PSilQ and C) PEG-RR-PpIX-PSilQ are incubated for 24 hours in fibroblast cultures (HDFn, blank) and murine melanoma (B16-F10, in gray).

Source: By the author.

It was detected that, when cells are exposed to Ctrl-PpIX-PSilQ solutions and kept in the dark, cell viability of both strains remained unaffected. However, after their irradiation, a dose-dependent behavior was verified, with the highest concentrations showing the greatest damage to cell viability. In addition, it is suggested that healthy cells do not show a reduction in their viability values up to 150 µg/mL solutions are applied, which results in almost 20% of viable cells. Nonetheless, for melanoma cells, the lower nanoparticles concentration was able to promote cell death of almost 70%, showing the B16-F10 cell line greater susceptibility to nanoparticles-mediated PDT. A similar behavior was observed with RR-PpIX-PSilQ nanoparticles, but fibroblast cultures exhibit a reduction in their cell viability for 50 µg/mL solutions, which remain close to 85%. Interestingly, when healthy cells are exposed to PEG-RR-PpIX-PSilQ nanoparticles, it was noticed that fibroblasts did not show a reduction in their cell viability values even after PDT, and that melanoma cells are susceptible to the nanoparticle cytotoxicity (with no light exposure).

The results showed the potential of nanoparticles for PDT, with selectivity being achieved using lower concentrations of these systems in *in vitro* studies. Free PpIX has shown efficacy comparable to that of the nanostructures, but displayed increased cytotoxicity, which is an unsedireble side effect.

4.8.4 ROS Production

To determine if the observed cell damage was promoted by PDT, experiments were conducted to detect substances that are known to be produced by the forementioned technique and that are involved in the oxidation of important cell structures and biomolecules. ROS production was assessed using H2DCFDA, a cell-permeant probe that initially presents no fluorescence. After cell uptake and cleavage by intracellular species, it becomes fluorescent in the presence of ROS, with an emission peak around 520 – 530 nm.

Initially, differences in ROS generation levels after cell exposure to nanoparticles and free PpIX for 24 hours were evaluated in breast cancer cultures. In figure 14 it is observed that neither the culture media nor DMSO promoted significant changes in ROS production, in the presence or absence of light. Free PpIX showed a pronounced increase on ROS generation upon irradiation, suggesting cell death was promoted by PDT. However, the greatest ROS production

was verified in samples exposed to RR-PpIX-PSilQ nanoparticles, which almost displayed a threefold increase on fluorescence signal when compared to the one yielded by cells that underwent PpIX-mediated PDT. This data suggests that, despite free PpIX presents enhanced internalization, when compared to the nanosystem, ROS production upon irradiation is not as efficient as RR-PpIX-PSilQ's. This is due, possibly, to the elevated number of PpIX molecules inside the cells, which may lead to PpIX aggregation and quenching, resulting in lower ROS production. Nonetheless, cell death is comparable among these samples.

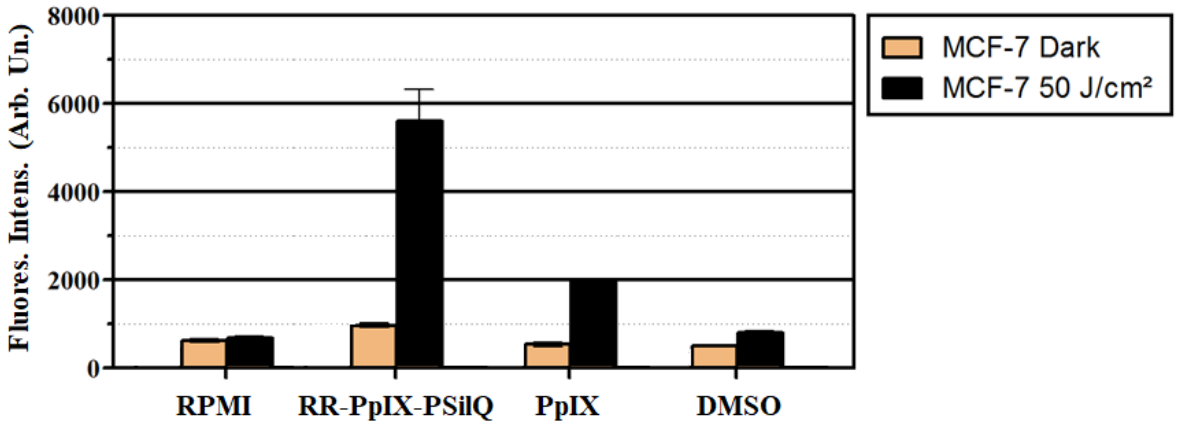

Figure 14 - ROS production in breast cancer cells in the absence (orange bars) or presence (black bars) of 630 nm.

Source: By the author.

To evaluate tumor and healthy cells ROS production upon RR-PpIX-PSilQ-mediated PDT, melanoma cell cultures and fibroblast cultures were submitted to the same experimental protocol. Figure 15 shows fibroblasts display a slight increase in ROS production uoon irradiation, with melanoma cells showing a significant increase after PDT, with approximately a 5-fold enhance in the fluorescence intensity when compared to the group that remained protected from light. This information correlates with the enhanced uptake described in section 4.7.2.

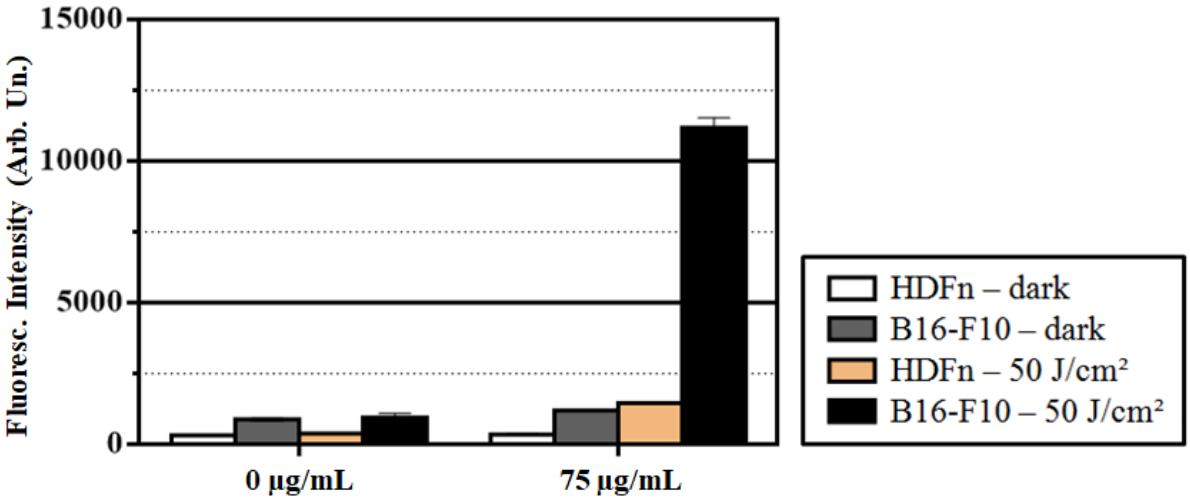

Figure 15 - ROS production in breast cancer cells in the absence (orange bars) or presence (black bars) of 630 nm.

Source: By the author.

5 LIPOSOMES

5.1. Membrane Fusogenic Liposomes

In 2016, Dr. Juliana Cancino-Bernardi (Chemistry Institute of the Alfenas Federal University - UNIFAL) and her student, Gabriela Mayr Reyes, established a methodology for PpIX encapsulation in membrane fusogenic liposomes (FAPEP Process number 2016/11890-5) at the Nanomedicine and Nanotoxicology Group (GNano, São Carlos Institute of Physics, University of São Paulo)(67). Through a collaboration, 22.5 µg/mL stock solutions of MFL samples with and without PpIX (blank samples) were freshly prepared before each experiments. Briefly, to synthetize 4 mL of each liposome, stock samples of polymers and PpIX were added to glass flasks in the following proportions:

a) blank MFLs: 100 µL of 10 mg/mL PEG solution, 480 µL of 10 mg/mL DMPC solution, 133 µL of 10 mg/mL DOTAP solution and 900 µL of chloroform with 10 % DMSO (v/v). All solutions were prepared in chloroform.
b) MFL-PpIX: 100 µL of 10 mg/mL PEG solution, 480 µL of 10 mg/mL DMPC solution, 133 µL of 10 mg/mL DOTAP solution and 900 µL of 100 µg/mL PpIX solution with 10 % DMSO (v/v). All solutions were prepared in chloroform.

The samples were homogeneously agitated using a magnetic stirrer for 20 minutes. The flasks were covered with punctured parafilm and remained 12-24 hours at room temperature, protected from light, to dry. After complete chloroform evaporation, the films were hydrated in PBS and homogenized with a magnetic stirrer for 20 minutes. Homogeneous liposomes were obtained using an extrusion apparatus at 40 °C with a polycarbonate membrane (pore size: 100 nm). After 20 cycles, the liposomes were stocked at room temperature and protected from light.

5.2 Material and Methods

5.2.1 Reagents

DMSO, PBS, MTT, DMEM and RPMI 1640 culture media with and without red phenol, FBS, H2DCFDA and cell lines (B16-F10 and A-431 were used as tumor cell line models, and HDFn was used as healthy cell line model) are thoroughly described in section 4.2.1. PEG (1,2-

distearoyl-sn-glycero-3-phosphoethanolamine-N-[methoxy(polyethylene glycol)-2000] ammonium salt, catalog number 800120, Avanti Polar Lipids, Inc., Alabaster, Alabama, USA), DMPC (1,2-dimyristoyl-sn-glycero-3-phosphocholine, catalog number 850345, Avanti Polar Lipids, Inc.) and DOTAP (1,2-dioleoyl-3-trimethylammonium-propane, catalog number 890890, Avanti Polar Lipids, Inc.) were kindly provided by the Nanomedicine and Nanotoxicology Group. Filter supports (catalog number 610014, Avanti Polar Lipids, Inc.) and polycarbonate membranes (pore size: 0.1 µm, diameter: 19 mm, Nucleopore Track-Etch Membrane, catalog number 800309, Whatman, Little Chalfont, Buckinghamshire, UK) were purchased from Sigma-Aldrich.

5.2.2 PpIX Uptake

To determine PpIX internalization when encapsulated by MFLs, studies were performed with an inverted fluorescence micocroscope (Zeiss Axio Observer.Z1, Zeiss) and flow cytometry (Accuri C6 Plus flow cytometer). Initially, melanoma cells (B16-F10) and fibroblasts (HDFn) were evaluated to assess differences between tumor and healthy cells uptake for both free PpIX and MFL-PpIX. Briefly, cells were seeded 24-well plates at a density of 10^5 cells/mL in DMEM supplemented with 10 % FBS. After cell adhesion (18-24h in a humidified incubator at 37 ºC and 5% CO_2 atmosphere) MFL-PpIX and the free PS (with a final PpIX concentration of 1.5 and 15 µg/mL, prepared in phenol-free DMEM supplemented with 10% FBS) were added to the plates, Cells were exposed to the samples for 24 hours at 37ºC and 5% CO_2 atmosphere in a humidified incubator.

For fluorescence mycorscopy analyses, cells were carefully washed with PBS twice and images were acquired using 350 ± 20 nm as excitation and using a 400 nm long pass filter for emission collection. For flow cytometry assessment, cells were dissociated from the plates, washed twice, resuspended in PBS and evaluated using the FL-3 channel (488 nm excitation with 670/LP filter detection). Background fluorescence was considered as the control group fluorescence (cells that weren't exposed to PpIX/MFL-PpIX). The same experiments were conducted with non-melanoma cells (A-431) and fibroblasts, evaluating lower incubation times (1 and 4 hours exposure) and lower PpIX concentration (1 µg/mL).

5.2.3 *In vitro* PDT Assays

In order to compare the MFLs efficacy in PDT to PSilQs, similar experimental parameters to the ones described in section 4.5 were assessed for the liposomes. Briefly, melanoma cells and fibroblasts weres seeded (10^5 cells/mL in RPMI 1640 supplemented with 5% SFB) in 96-well plates and kept in a humidified incubator for 24 hours. The supernatant was replaced by phenol-free DMEM supplemented with 10% FBS (control group) and solutions of blank MFLs, MFL-PpIX and free PpIX (with 1.5, 7.5 and 15 μg/mL as final PpIX concentration), with cell exposure to the samples for 24 hours. After careful sample washing with PBS, 50J/cm² (630 nm) was used to irradiate one plate, while dark control groups remained protected from light. To obtain cell viability, MTT was used. To evaluate the impact and selectivity of MFLs to tumor cells, experiments were performed using non-melanoma skin cancer cells and fibroblasts. Lower light fluence (20, 40 and 50 J/cm²), PpIX concentration (0.1, 0.5 and 1 μg/mL) and incubation times (1 and 4 hours) were assessed using the previously described methodology.

5.2.4 ROS Quantification

ROS production was also evaluated when tumor cells and healthy cells were submitted to free PpIX and PpIX-mediated PDT using H2DCFDA as described in section 4.6. Briefly, 10^5 melanoma cells or fibroblasts/mL were seeded 24 hours prior the experiments in in 96-well plates and incubated for 24 hours with a final concentration of PpIX corresponding to 1.5 and 15 μg/mL for both MFL-PpIX and the free PS. 30 minutes before light exposure, cells were carefully washed and incubated with 10 μM H2DCFDA working solution, and washed immediately before irradiation with 630 nm - 50 J/cm² (dark control groups remained protected from light). Fluorescence intensity was quantified with excitation/emission set as 485/520 nm. The same experimental protocol was used to assess non-melanoma skin cancer cells ROS production when cells were exposed for 1 and 4 hours to a final PpIX concentration of 0.1 and 1 μg/mL in MFL, MFL-PpIX and free PpIX solutions and irradiated with 50 J/cm².

5.2.5 Statistical Analysis

As in chapter 4, cell viability results were expressed as the mean ± standard deviation. Groups were performed in triplicates and the experiments were repeated in three different occasions, resulting in n = 9 (with exception for PDT assays with lower PpIX/MFL-PpIX concentrations, exposure time and light fluence, which were repeated twice, resulting in n = 6). Statistical analysis was performed using GraphPad Prism 5, aplying one-way ANOVA (even for groups that did not present normal distributions, when the test was used outside its hypothesis) followed by Tukey's multiple comparison test. Statiscally significant differences were determined by comparisons displaying $p \leq 0.05$, indicated in the graph by *.

5.3 Results and Discussion

5.3.1 PpIX Uptake

PpIX internalization was studied initially over 24 hour incubation in tumor (melanoma) cells and in healthy (fibroblast) cells cultures using fluorescence microscopy and flow cytometry. In melanoma cells, it was observed a mild fluorescence intensity located mainly in cells borders when 1.5 µg/mL MFL-PpIX was used (figure 16A). Increasing PpIX concentration resulted in a slight increase on the fluorescence signal and localization: 15 µg/mL solutions resulted in a more homogeneous fluorescence spread throughout the cells cytoplasm. Free PpIX, however, displayed significant increase on the fluorescence intensity when comparing 1.5 and 15 µg/mL: 1.5 µg/mL resulted in low fluorescence signal, also located more consistently on cell borders. Increasing PpIX concentration to 15 µg/mL promoted elevated PpIX internalization, confirmed by intense fluorescence signal, mostly observed in cells cytoplasm (figure 16A, lower panels). When 1.5 µg/mL uptake was assessed by flow cytometry (figure 16B), a shift on the fluorescence signal was detected on the cell population that was exposed to MFL-PpIX towards higher fluorescence intensity. This indicates cells were able to interact with the liposomes, internalizing PpIX after 24 hours exposure. When free PpIX was used, it resulted in a less intense shift on cell population, indicating MFL-PpIX is more efficient to promote PpIX internalization in melanoma cells. The same behavior is not observed for 15 µg/mL, despite the cytotoxic effect on cell viability reducing the cell population (observed in

the PpIX cell population flattening in figure 16B, lower panel): cells present higher fluorescence intensity, displaying equal or more intense signal when compared to MFL-PpIX, corroborating the results observed in fluorescence microscopy. Therefore, free PpIX is more efficiently internalized by melanoma cells when compared to MFL-PpIX, and its cytotoxic effects become evident in flow cytometry assays. This effect was also observed in breast cancer cells (section 4.8.2) when RR-PpIX-PSilQ were studied, with the free PS presenting a homogeneous spread in cell cytoplasm.

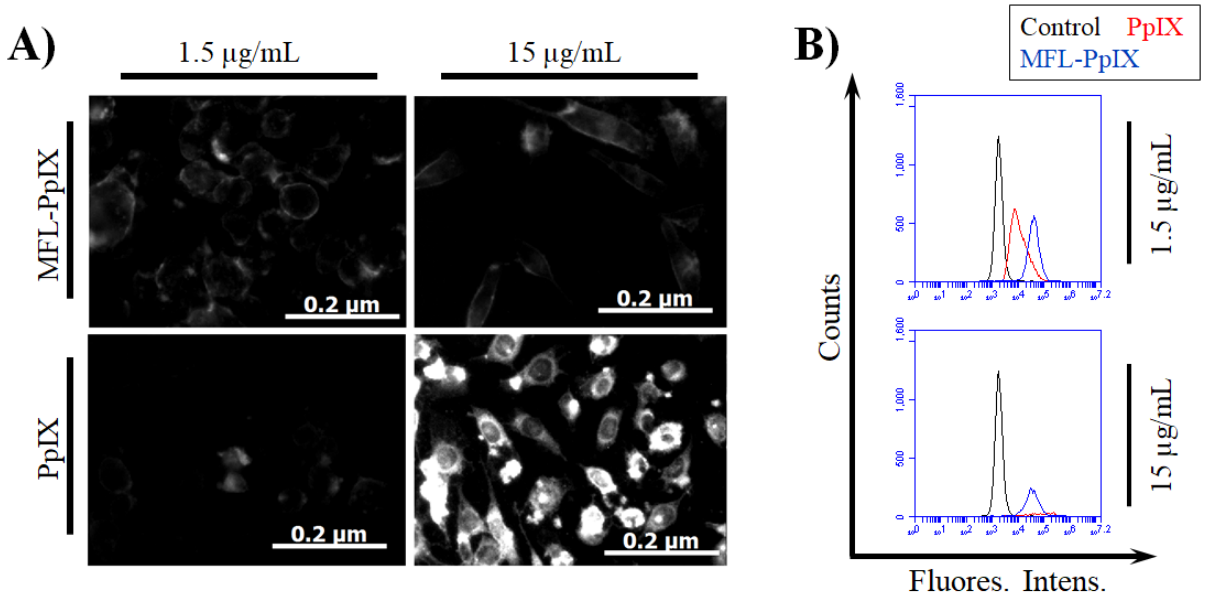

Figure 16 - MFL-PpIX and free PpIX uptake after exposure for 24 hours in melanoma cells evaluated by A) fluorescence microscopy (where fluorescence is displayed in white) and B) flow cytometry.

Source: By the author.

When MFL-PpIX and free PpIX uptake was evaluated in fibroblasts with fluorescence microscopy (figure 17A), it was observed that, for 1.5 µg/mL, the fluorescence intensity is mild, but is homogeneously spreaded across the cell cytoplasm when free PpIX is used. For MFL-PpIX, however, PpIX appear to concentrate in filaments, suggesting the MFLs might present affinity to the cytoskeleton fibers. To determine the exact location of MFL-PpIX, a technique such as LCSM is required, with z-stacking allowing a close look into different cell planes. When the PS concentration is increased, a fluorescence intensity increase is verified for both samples, but in larger scale for free PpIX. In flow cytometry, it was observed small differences between the population shift, when compared to cells that wasn't exposed to PpIX, promoted by the free PS or when encapsulated in MFLs for 1.5 µg/mL. This suggests that, for this

particular healthy cell line, liposomes present similar uptake efficiency when compared to free PpIX. The increase in concentration results in a small population shift towards higher fluorescence intensity when MFL-PpIX is assessed, with free PpIX displaying a more significant shift, reinforcing fluorescence mycrosocopy data.

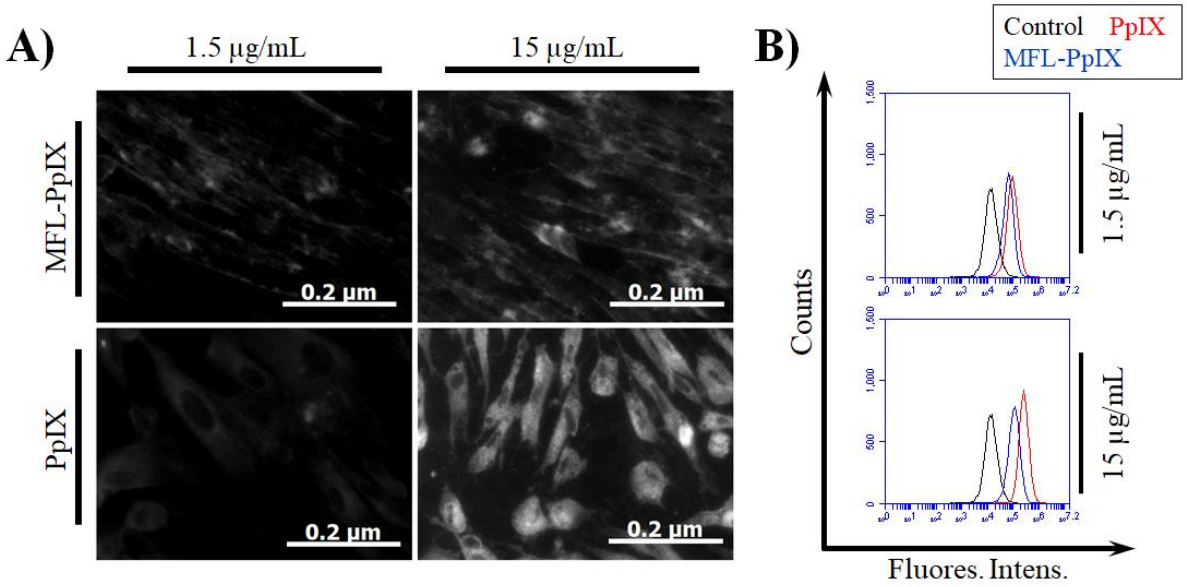

Figure 17 - MFL-PpIX and free PpIX uptake after exposure for 24 hours fibroblasts using A) fluorescence microscopy (where fluorescence is displayed in white) and B) flow cytometry

Source: By the author.

When incubation times and PpIX concentration were reduced (1 and 4 hours, 1 µg/mL), it was observed in fibroblasts a slight increase in the fluorescence intensity for both free PpIX and MFL-PpIX exposure (figure 18A). Flow cytometry assay showed a small percentage of cells showed PpIX internalization after 1 hour of exposure to MFL-PpIX, close to 1%. After 4 hours of incubation, the population that presented increased fluorescence intensity corresponded approximately to 6% (figure 18B). Free PpIX yielded higher percentages for both incubation times, with 20 and approximately 85% for 1 and 4 hours, respectively. This data relates to the previous observations when comparing free PpIX and nanoparticles uptake over extende incubation times, and shows that MFL-PpIX uptake is a slow process when compared to free PpIX, probably due the nature of the mechanisms that take part on the internalization of each sample.

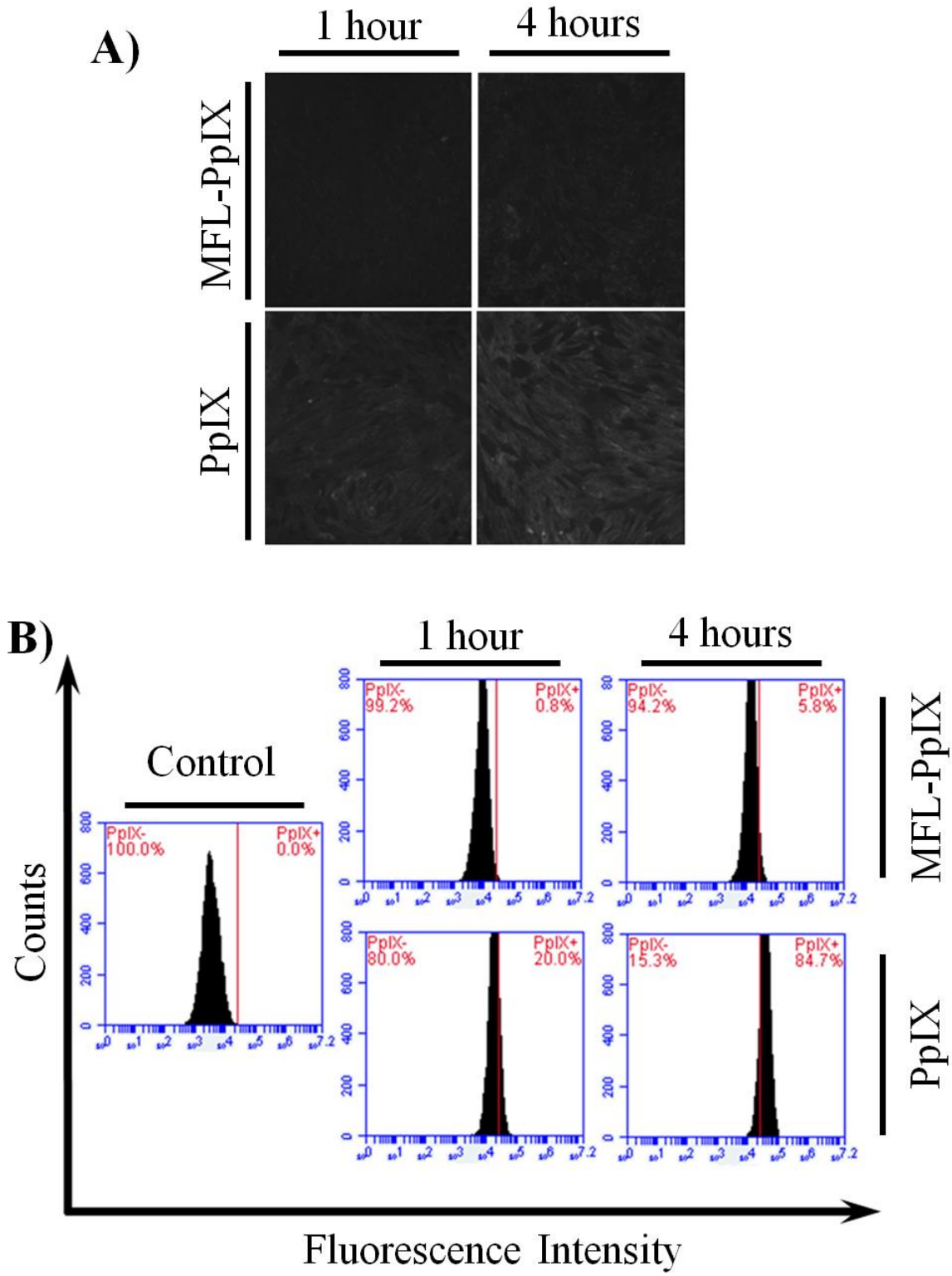

Figure 18 - MFL-PpIX and free PpIX uptake in fibroblasts (1 µg/mL, 1 and 4 hours) evaluated by A) fluorescence microscopy (where fluorescence is displayed in white) and B) flow cytometry.

Source: By the author.

For non-melanoma skin cancer cultures, fluorescence microscopy revealed similar uptake behavior to the one verified in fibroblasts cultures (figure 19A). However, increased PpIX uptake was highlighted in flow cytometry results: 9 and approximately 21% of cell population displaying elevated fluorescence signal when cells were exposed to MFL-PpIX for 1 and 4 hours, respectively. Cells exposed to free PpIX yielded high a percentage of the population (approximately 95%) presenting PpIX internalization after 1 hour of exposure. After 4 hours, this number increased to almost 99%. This is in accordance to what was expected, considering tumor cells have enhanced metabolism and increased uptake.

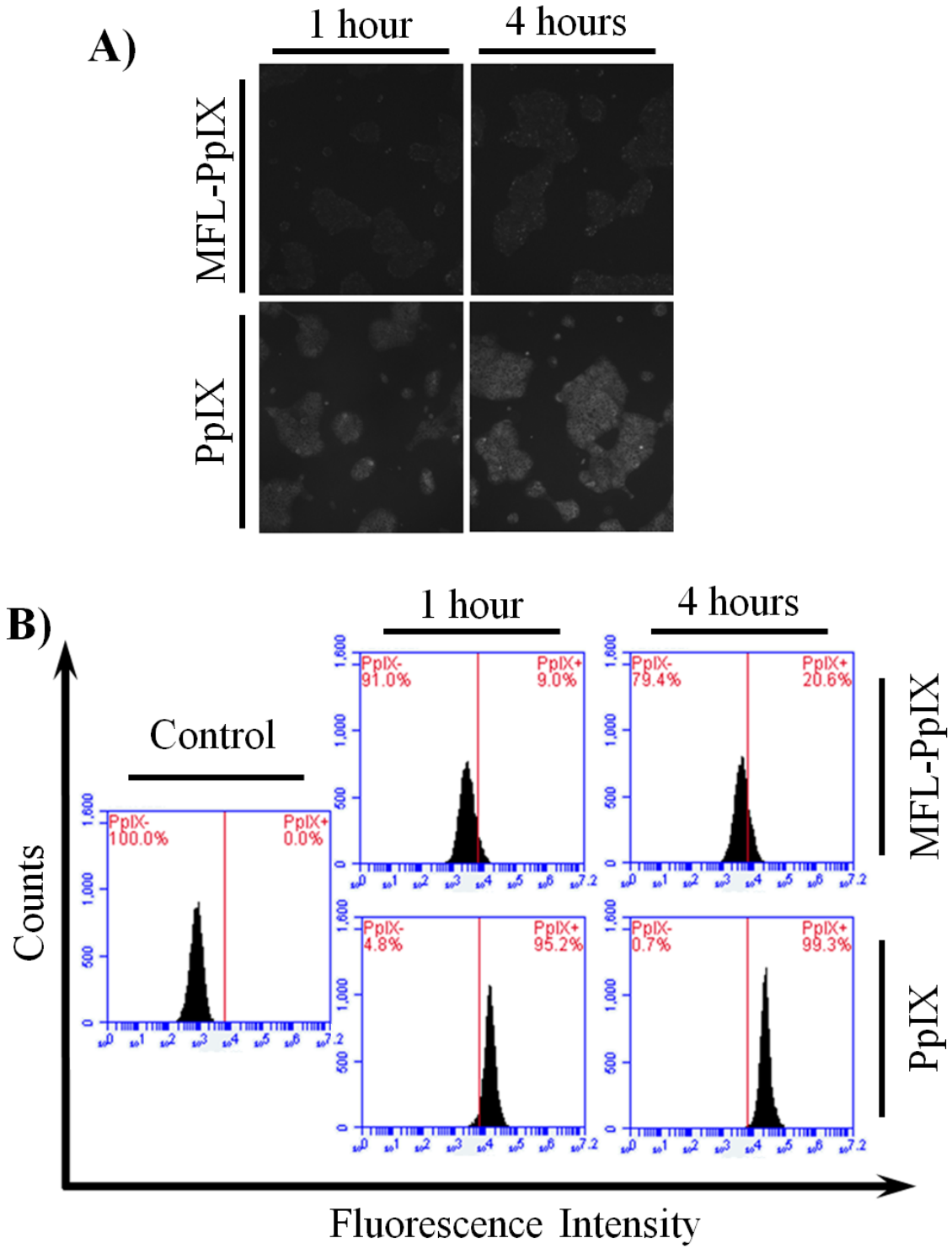

Figure 19 - MFL-PpIX and free PpIX uptake in non-melanoma skin cancer cultures (1 µg/mL, 1 and 4 hours) evaluated by A) fluorescence microscopy (where fluorescence is displayed in white) and B) flow cytometry.

Source: By the author.

5.3.2 PDT

To evaluate MFL-PpIX efficacy for *in vitro* PDT, experiments with melanoma cells were performed, incubating for 24 hours blank MFLs, MFL-PpIX and free PpIX with a final concentration of the PS corresponding to 1.5, 7.5 and 15 µg/mL. As it can be seen in figure 20, blank MFLs and MFL-PpIX display similar cytotoxicity to the melanoma cells, reducing cell viability in approximately 20%, indenpendently on the concentration. Free PpIX present similar effect on the cells up to 7.5 µg/mL, and 15 µg/mL solutions display higher impact on cell viability, that remained close to 55%. Upon irradiation, blank MFLs show no further damage on cell viability, revealing that the liposome formulation did not present photoactive properties, as it was expected. MFL-PpIX, however, display a drastic reduction on cell viability, with no dependence on the PpIX concentration: cell viability values were approximately 4% for all samples. Free PpIX results were very similar to MFL-PpIX, with almost complete decimation of melanoma cultures upon PDT. These data suggest that the studied concentrations might contain more PpIX than optimal concentration, due the absence of a dose-dependent behavior even when a tenfold increase on the concentration was assessed.

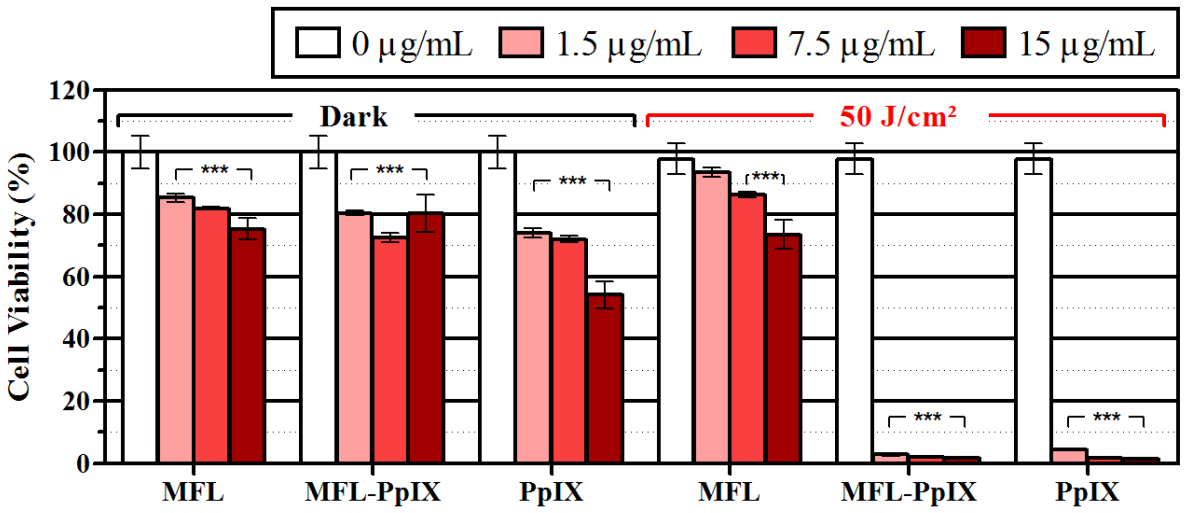

Figure 20 – Blank MFL, MFL-PpIX and free PpIX PDT in melanoma cultures after exposing cells for 24 hours to 1.5, 7.5 and 15 µg/mL. Results are displayed as mean values of cell viability, and *** indicates significant differences when compared to the control group (cells not exposed to MFLs or PpIX and protected from light), with $p \leq 0.005$.

Source: By the author.

To evaluate MFL-PpIX-mediated PDT in healthy cell cultures, the same parameters were tested in fibroblasts cultures. Blank MFLs displayed similar effects on cell viability when compared to melanoma cultures, yielding cell viability values of aproximately 80% and showing no dependence on MFL concentration (figure 21). MFL-PpIX, however, revealed a dose-dependent cytotoxicity, suggesting fibroblasts are more prone to PpIX cytotoxicity, even when the PS is encapsulated. This pattern is repeated in groups exposed to free PpIX,which, as seen in melanoma cultures, has similar cytotoxicity to MFL-PpIX up to 7.5 µg/mL. The highest concentration presents a reduction of almost 20% in cell viability when compared to MFL-PpIX, resulting in 40% of viable cells after 24 hours. When compared to melanoma cells, it is observed lower cell viability of the healthy cells, reinforcing the higher susceptibility of these cells to PpIX cytotoxicity. In PDT groups, blank MFLs present the same cell viability values, corroborating the absence of liposomes photoactivity due the absence of impact on cell viability upon irradiation. MFL-PpIX and free PpIX, however, display huge impact on cell viability after exposure to 630 nm with 50 J/cm², as it was also observed in the previously described results in melanoma cells.

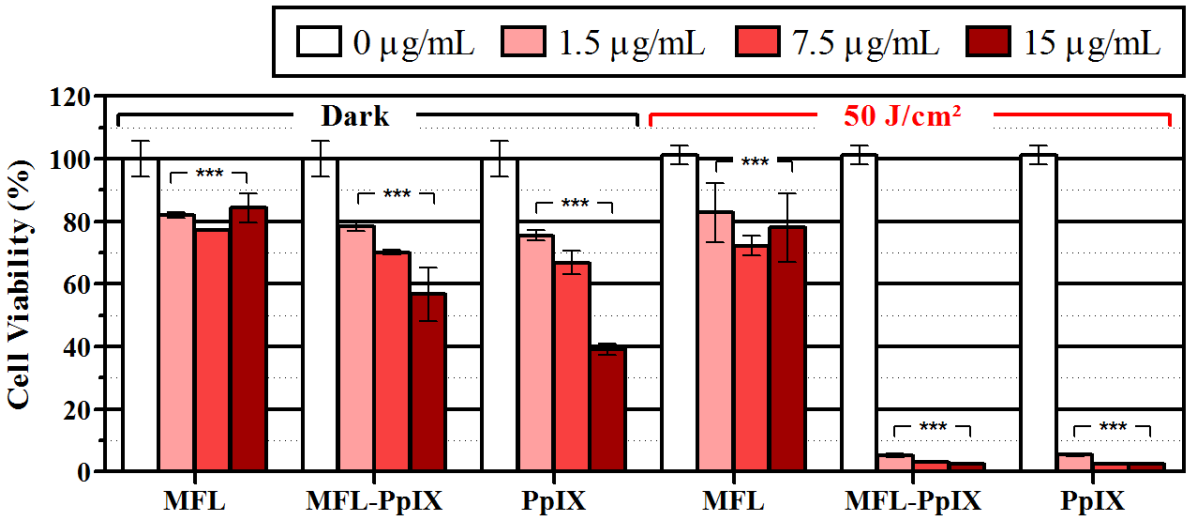

Figure 21 – Blank MFL, MFL-PpIX and free PpIX PDT in fibroblasts cultures after exposing cells for 24 hours to 1.5, 7.5 and 15 µg/mL. Results are displayed as mean values of cell viability, and *** indicates significant differences when compared to the control group (cells not exposed to MFLs or PpIX and protected from light), with $p \leq 0.005$.

Source: By the author.

As no dose-dependence was verified for the chosen experimental parametes so far, lower incubation times (1 and 4 hours) PpIX concentration (0.1, 0.5 and 1 µg/mL) and light

fluences were assessed in tumor cells and healthy cells. When non-melanoma skin cancer cultures were exposed to free PpIX for 1 hour, no cytotoxicity was observed when samples remained protected from light (figure 22). Upon irradiation, a dose-dependent pattern was observed for both PpIX concentration and light fluence: it was verified that 5 J/cm² was able to promote cell death on 60% of the population only when 1 µg/mL was used. 20 J/cm² promoted cell damage when 0.5 and 1 µg/mL solutions were used, with light fluence increase resulting in enhanced cell death. When assessing 50 J/cm², even the lowest PpIX concentration was able to promote a decrease on cell viability corresponding to approximately 50%. When cells were exposed for 4 hours to free PpIX, similar results were obtained, with a mild enhance on cell damage. This suggests that, over time, cells are able to internalize increased amounts of the free PS, enhancing the photodynamic damage, which is in accordance to the data produced by previously described uptake assays. Considering 20 J/cm² did not display efficient cell death rates, MFL-PpIX experiments were conducted with 1 and 4 hour incubation of 0.1, 0.5 and 1 µg/mL and ligh fluences of 20 and 50 J/cm². No cytotoxicity was observed when cells weren't exposed to 630 nm, and the same dose-dependent behavior thar was veririfed in free PpIX assays was also observed for MFL-PpIX. However, when comparing the effect of nanostructured PpIX to the free PS on cell viability, non-melanoma skin cancer show higher susceptibility to PDT when MFL-PpIX is used. For 1 hour of 0.1 µg/mL incubation, free PpIX reduced didn't show any cell damage when exposed to 20 J/cm². For samples exposed to MFL-PpIX under the same conditions, cell viability values are reduced to approximately 60 %. The increase on incubation time becomes irrelevant (for this particular scale, 1 and 4 hours) when MFL-PpIX solutions of 0.5 µg/mL (or greater) are applied, almost completely decimating the cell population (viability values ranging from 3 to 5%).

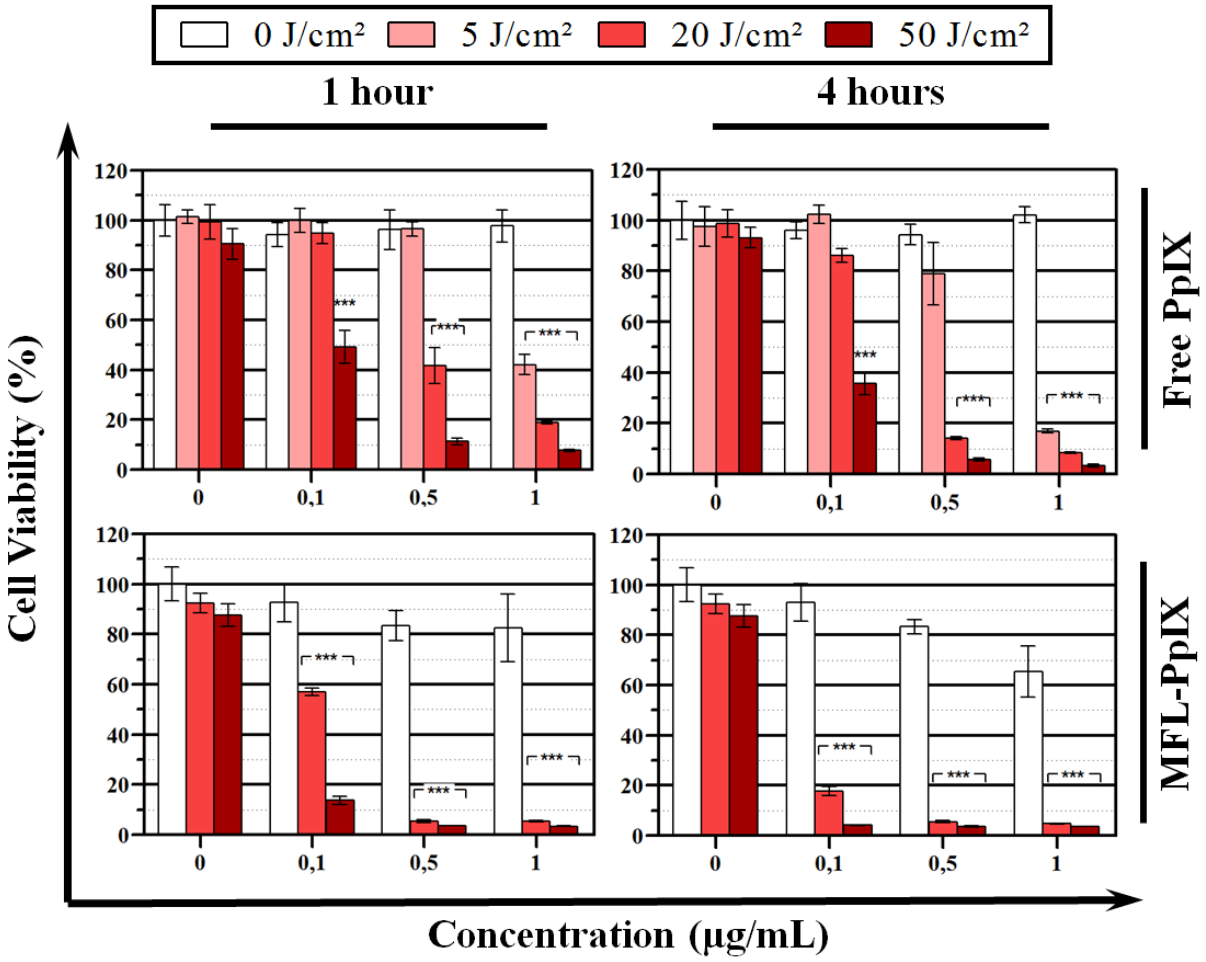

Figure 22 – Free PpIX and MFL-PpIX-mediated PDT in non-melanoma skin cancer cultures after exposing cells for 1 and 4 hours to 0.5, 0.5 and 1 µg/mL and using 20, 40 and 50 J/cm² to irradiate the samples. Results are displayed as mean values of cell viability, and *** indicates significant differences when compared to the control group (cells not exposed to MFLs or PpIX and protected from light), with $p \leq 0.005$.

Source: By the author.

With 1 hour exposure to free PpIX, healthy cells cultures showed a dose-dependent profile mainly to PpIX concentration: no cell viabiality reduction when 0.1 µg/mL solutions were evaluated (figure 23). When the PS concentration was increased to 0.5 µg/mL, cell survival values were approximately 75 and 65% when 20 J/cm² was delivered to the plates, with 50 J/cm² resulting in 30% of viable cells for 1 µg/mL incubation. Enhancing exposure time to the PS for 4 hours, fibroblasts become prone to PDT with the tested concentrations, with a dose-depent behavior on light fluence becoming evident when cells are incubated with 1 µg/mL solutions.

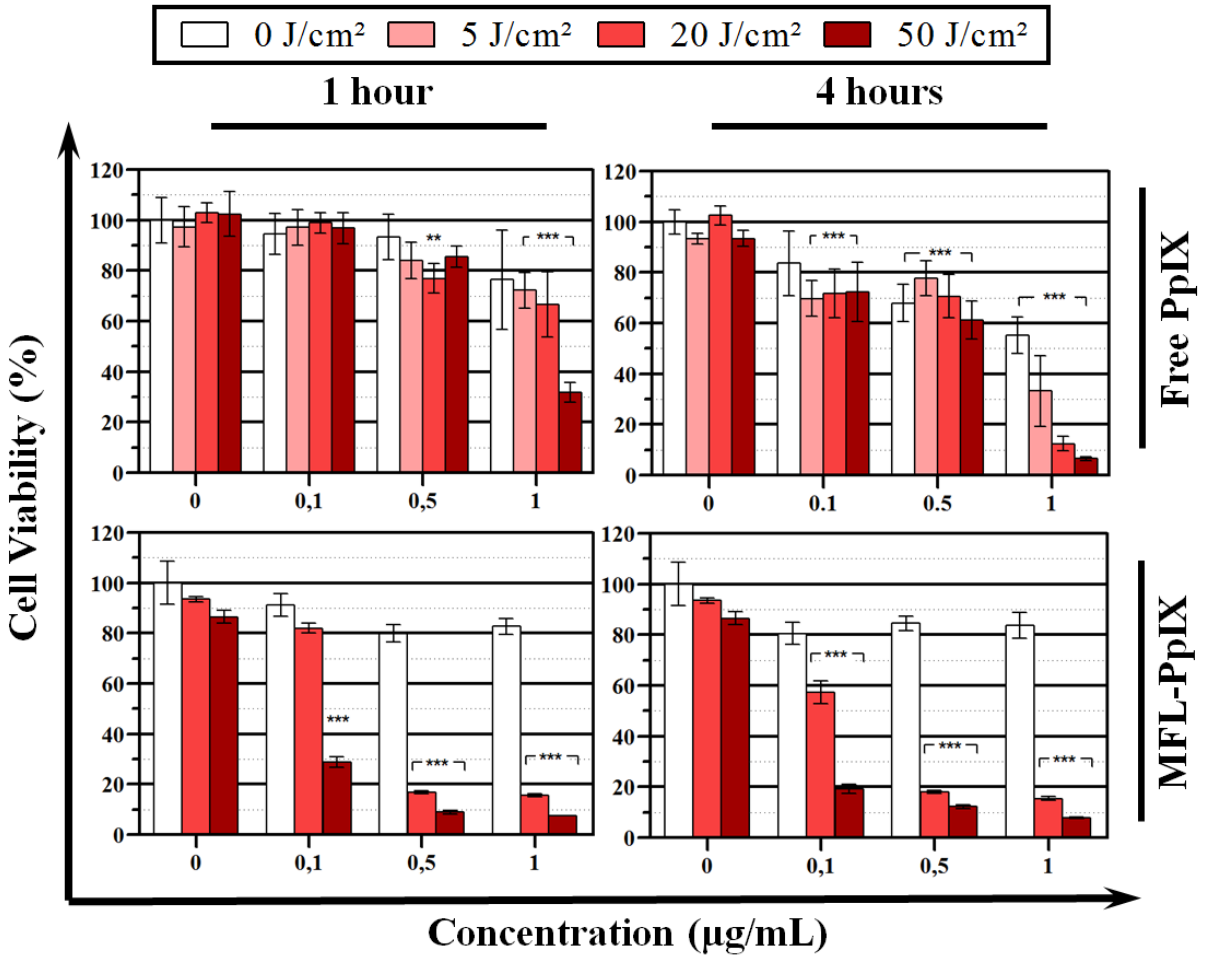

Figure 23 – Free PpIX and MFL-PpIX-mediated PDT in fibroblasts cultures after exposing cells for 1 and 4 hours to 0.5, 0.5 and 1 µg/mL and using 20, 40 and 50 J/cm² to irradiate the samples. Results are displayed as mean values of cell viability, with ** and *** indicating significant differences when compared to the control group (cells not exposed to MFLs or PpIX and protected from light), with $p \leq 0.05$ and $p \leq 0.005$, respectivelly.

Source: By the author.

Comparing tumor cell and healthy cells responses to free PpIX-mediated PDT, it is observed that non-melanoma cells present higher susceptibility to PDT damage than fibroblasts, most probably due the differences in PpIX uptake. As described in section 5.3.1, with 1 hour exposure, most of non-melanoma cells were able to internalize the free PS, while only 20% of fibroblasts present PpIX fluorescence. The difference between positively marked cells for PpIX between both cell lines is greatly reduced after 4 hours, when approximately 84% of healthy cells show PpIX incorporation. In particular, damage selectivity was greatly achieved when cells were exposed to 0.5 µg/mL for 1 hour, resulting in approximately 80% of fibroblasts

remaining viable after PDT, but non-melanoma skin cancer displayed cell survival of 40 and 10% when irradiated with 20 and 50 J/cm², respectively.

When MFL-PpIX were assessed in fibroblasts, PDT becomes much more effective, when compared to the free PS. Almost no difference is observed when incubation time is increased, except for the lowest concentration. When 0.1 µg/mL MFL-PpIX is incubated for 1 hour, 20 J/cm² PDT displays no effect on cell viability, however, after 4 hours, cell viability values decrease to approximately 57%. Comparing cell damage promoted by MFL-PpIX-mediated PDT to the observed results in non-melanoma skin cancer assessment, tumor cells present more prone to cell damage than healthy cells, with the enhanced photoxicity due to differences in sample uptake, as it was expected due tumor cells fast metabolism and data obtained in fluorescence microscopy/flow cytometry. MFL-PpIX selectivity to tumor cells was verified only when cells were exposed to 0.1 µg/mL for 4 hours and irradiated with 20 J/cm²: fibroblasts cultures yielded viability values close to 60% while non-melanoma skin cancer cells presented almost 18% of viable cells after PDT.

5.3.3 ROS Production

As described in section 4.8.4, PDT cytotoxicity may result from ROS generation upon irradiating photoactive substances. Using H2DCFDA, we assessed if, as seen for the PSilQ nanopplatform, the damage promoted by liposome-carried PpIX-mediated PDT was due the photodynamic process. We first evaluated PDT using a final concentration of PpIX corresponding to 1.5 and 15 µg/mL of both PpIX and MFL-PpIX incubated for 24 hours. 50 J/cm² were delivered to melanoma cell cultures and fibroblasts.

In melanoma cells (B16-F10), when cells remain protected from light exposure, no significant differences on ROS levels are detected in any sample (figure 24). Upon irradiation with 630 nm (50 J/cm²), basal levels of ROS are increased, with blank MFL displaying no significant effect on ROS production. Cells exposed to PpIX, however, showed an increase on these species generation, with fluorescence intensity displaying a non-linear direct dependence on PpIX concentration. ROS production was more extensively produced on cells exposed to 15 µg/mL MFL-PpIX, despite increased uptake being observed when free PS is used. This may be due the proximity of the molecules inside the cells, with increased PpIX concentrations in the

cytoplasm resulting in molecules close to each other. Tighly packed molecules may lead to aggregation and quenching, which could explain lower ROS production. But as it was seen in section 5.3.2, no significant difference in cell viability was produced when comparing MFL-PpIX and free PpIX, considering almost complete cell death was achieved for all concentrations in both samples. This reinforces the idea that optimal PpIX concentration may be lower than the ones initially assessed.

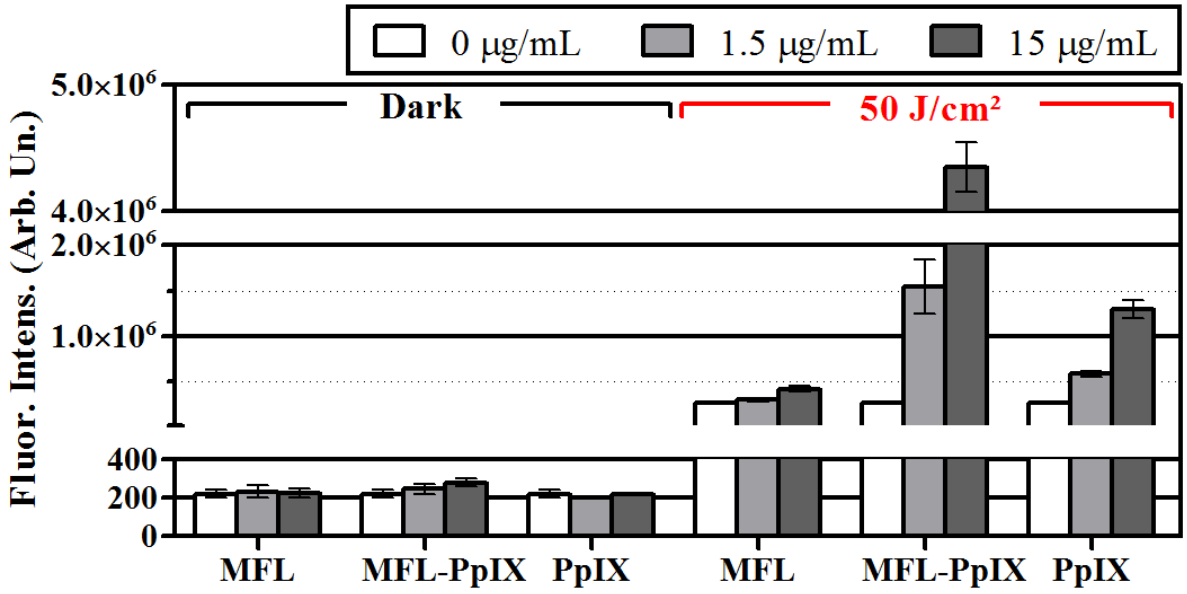

Figure 24 – Fluorescence intensity measurement for ROS production quantification in melanoma cells exposed to blank MFL (MFL), MFL-PpIX and free PpIX after incubation for 24 hours. PDT and phototoxicity groups were exposed to 630 nm, with a light fluence of 50 J/cm².

Source: By the author.

In experiments involving fibroblastos, the absence of variations on ROS levels when samples are kept in the dar kis also observed, independently on PpIX concentration (figure 25). Light exposure to the previously described parameters resulted on a slight increase on ROS production when cells are exposed to blank MFLs, as it was also verified in melanoma cells. Higher H2DCFDA fluorescence intensity values were observed when PpIX concentration was increased, for both MFL-PpIX and free PpIX, with liposomes presenting greater levels of ROS production, as it was also observed in tumor cells cultures. When compared to melanoma cells, fibroblastos show lower fluorescence signal, which are explained by the reduced cell number of healthy cells after seeding when compared to melanoma cells, due to tumor cells presenting faster growth rates, and the increased PpIX uptake verified in tumor cells. Lower ROS

production, however, didn't lead to lower PDT efficacy, with fibroblasts and melanoma viability presenting no significant differences.

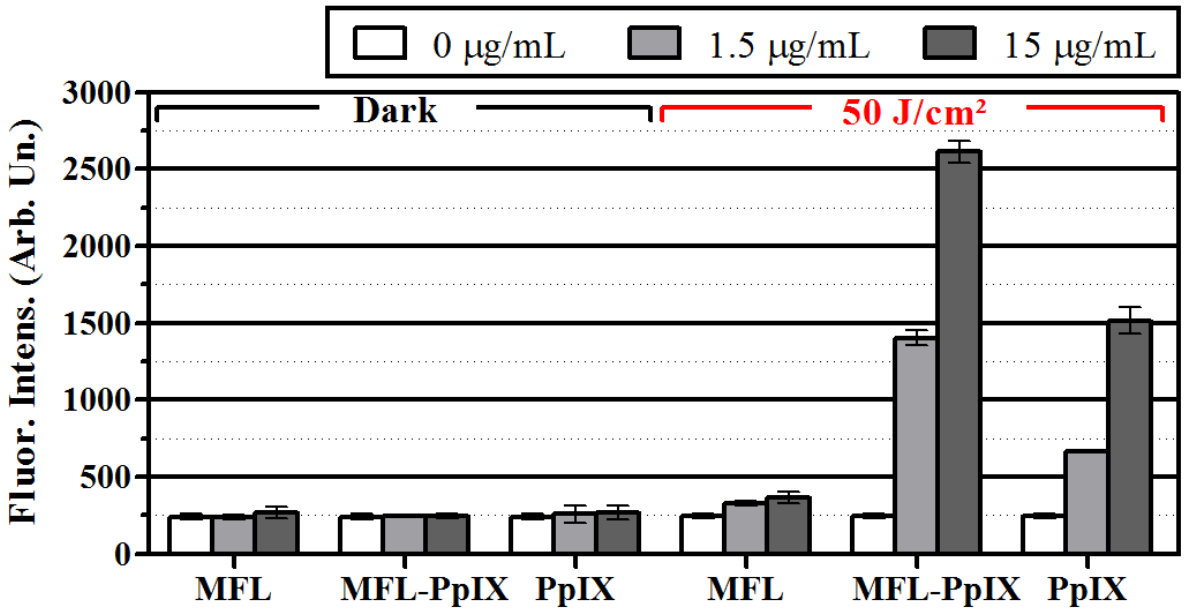

Figure 25 – Fluorescence intensity measurement for ROS production quantification in fibroblasts exposed to blank MFL (MFL), MFL-PpIX and free PpIX after incubation for 24 hours. PDT and phototoxicity groups were exposed to 630 nm, with a light fluence of 50 J/cm².

Source: By the author.

The absence of MFL-PpIX selectivity to tumor cells and the lack of a dose-dependent profile on PpIX concentration may suggest that optimal PDT parameters might be attained using lower incubation times, light fluence and PpIX concentration. PDT assays revealed MFL-PpIX-mediated PDT is more efficient when compared to treatment using free PpIX, and showed non-melanoma skin cancer cells are more prone to PDT damage than fibroblasts. Therefore we assessed ROS production in non-melanoma skin cancer cells when cells were exposed for 1 and 4 hours to the lowest and higher concentration (0.1 and 1 µg/mL) and irradiated with 50 J/cm². When exposure occurred for 1 hour, it was observed a slight difference in ROS levels when cells weren't exposed to light when blank MFLs were used, including µg/mL when samples were exposed to light (figure 26). But a significant increase on ROS production was attained when 1 µg/mL solutions of MFL-PpIX and free PpIX were used. No further enhancement in these molecular species generation was observed when cells were exposed to the samples for 4 hours, which is in accordance with the cell death promoted by these parameters, described in section 5.3.2, that presented similar viability values for both 1 and 4 hour exposure.

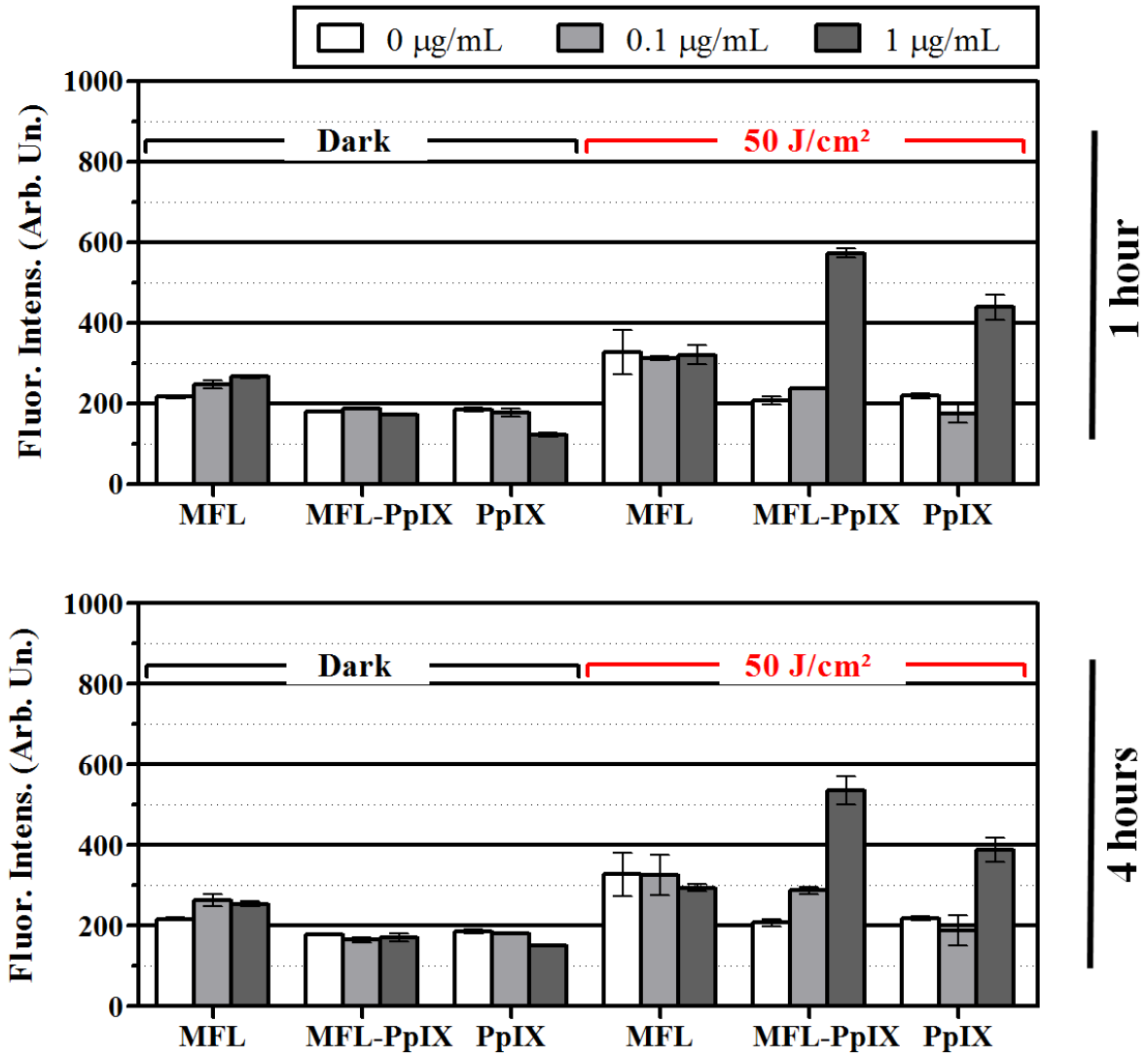

Figure 26 – Fluorescence intensity measurement for ROS production quantification in fibroblasts exposed to blank MFL (MFL), MFL-PpIX and free PpIX concentrations, corresponding to a final PpIX concentration of 0.1 and 1 0.1 and 1 µg/mL, after incubation for 1 and 4 hours. PDT and phototoxicity groups were exposed to 630 nm, with a light fluence of 50 J/cm².

Source: By the author.

6 CONCLUSION

Cancer is among the biggest causes of mortality in the world and its incidence continues to increase year after year, making it necessary to perpetuate investigations of alternative or supporting techniques for the treatment of this set of diseases. The combination of the oxidative damage of PDT with the improvement in FSs delivery to the treatment target that nanotechnology provides can potentiate the treatment effects, and allow tumors located in deeper tissues to be treated with this technique. Thus, it was proposed to evaluate the potential of redox-responsive silica nanoparticles (PSilQ nanoparticles) and membrane fusogenic liposomes (MFLs) carrying PpIX for PDT. The effect of different solventes on PSilQ nanoparticles, nanostructures uptake and their phototoxicity have been evaluated.

It was found that, for both PpIX and nanoparticles, the use of culture media or PBS for its preparation favors its aggregation, however images from confocal microscopy and other techniques evaluating PpIX fluorescence, as well as the intensity of its signal, showed internalization by breast cancer cells after 24 hours of exposure. It was observed that, when free PpIX concentration matches the corresponding PpIX concentration carried by the nanoparticles are incubated with the cells, there is a greater incorporation of the PS, which is distributed almost homogeneously throughout cell cytoplasm. PSilQ nanoparticles incubation reveals lower PpIX internalization and exhibits aggregates in the cytoplasm. Despite these distinctions, phototoxicity studies have shown that the efficiency of free PpIX and PSilQ nanoparticles, in *in vitro* tests, are comparable but with the advantage that the nanostructured PpIX presented lower toxicity in the dark, compared to the free PS. It is also possible to modulate the PSilQ selectivity to murine melanoma cells, when compared to fibroblasts, by using lower nanocarrier concentrations. ROS quantification assays revealed both free PpIX and RR-PpIX-PSilQ promote ROS production when exposed to 630 nm (50 J/cm^2), with the nanoparticles producing larger quantities. This suggests that when PpIX is nanostructured, lower amounts of the PS is internalized but the molecules are found inside the cells mainly in its monomeric form. Upon irradiation, the absence of aggregation results in increased ROS production, when compared to PpIX. In its free form, PpIX is more efficiently internalized but yields lower ROS production, probably due the close proximity of the molecules and aggregation, which may lead to quenching. Liposomal PpIX also showed higher susceptibility of tumor cells to PDT, and displayed increased ROS production when compared to free PpIX. When compared to PSilQ,

MFLs showed similar effects on cell viability upon irradiation with lower PpIX concentrations and lower incubation times.

In general, *in vitro* assays revealed it is possible to promote selective cell damage to tumor cell lines varying PpIX concentration and incubation time. Both nanostructures displayed similar efficacy for *in vitro* anti-tumor PDT when compared to free PpIX, presenting lower cytotoxicity to the cells when protected from light. This suggests PSilQ and MFLs may present increased PDT efficacy in pre-clinical studies when compared to the free PS, where more complex effects take place, such as opsonisation and corona protein, that tend to reduce treatment efficacy.

REFERENCES

1 STEWART, B.; WILD, C. P. (ed.). **World cancer report 2014**. Lyon: WHO, 2014.

2 HANAHAN, D.; WEINBERG, R. A. The Hallmarks of cancer. **Cell,** v. 100, n. 1, p. 57-70, 2000.

3 HANAHAN, D.; WEINBERG, ROBERT, A. Hallmarks of cancer: the next generation. **Cell,** v. 144, n. 5, p. 646-674, 2011.

4 ORGANIZAÇÃO MUNDIAL DA SAÚDE. **Cancer**: fact sheet n°297. 2015. Available from: http://www.who.int/mediacentre/factsheets/fs297/en/. Accessible at: 9 May 2015.

5 MEDICAL NEWS TODAY. **What is a tumor?.** 2014. Available from: http://www.medicalnewstoday.com/articles/249141.php. Accessible at: 10 May 2015.

6 ORGANIZAÇÃO MUNDIAL DA SAÚDE. **Câncer**. Available from: http://www.who.int/cancer/en/. Accessible at: 15 Sept. 2017.

7 ORGANIZAÇÃO MUNDIAL DA SAÚDE. **Cancer fact sheet**. 2017. Available from: http://www.who.int/mediacentre/factsheets/fs297/en/. Accessible at: 12 Aug. 2017.

8 BRASIL. Ministério da Saúde. Instituto Nacional de Câncer. **Estimativa 2014**: incidência de câncer no Brasil. Rio de Janeiro: INCA, 2014. 124 p.

9 BRASIL. Ministério da Saúde. Instituto Nacional de Câncer. **Estimativa 2016**: incidência de câncer no Brasil. Rio de Janeiro: INCA, 2015.

10 SIMÕES, M. C. F.; SOUSA, J. J. S.; PAIS, A. A. C. C. Skin cancer and new treatment perspectives: a review. **Cancer Letters,** v. 357, n. 1, p. 8-42, 2015.

11 BRASIL. Ministério da Saúde. Instituto Nacional de Câncer. **Tipos de câncer**: pele não melanoma. Available from: http://www2.inca.gov.br/wps/wcm/connect/tiposdecancer/site/home/pele_nao_melanoma. Accessible at: 10 Oct. 2017.

12 BRASIL. Ministério da Saúde. Instituto Nacional de Câncer. **Tipos de câncer**: pele melanoma. Available from: http://www2.inca.gov.br/wps/wcm/connect/tiposdecancer/site/home/pele_melanoma. Accessible at: 14 Oct. 2017.

13 VAZQUEZ, V. D. L. *et al*. Melanoma characteristics in Brazil: demographics, treatment, and survival analysis. **BMC Research Notes,** v. 8, n. 1, p. 1-9, 2015.

14 BRASIL. Ministério da Saúde. Instituto Nacional de Câncer. **Tipos de câncer**: mama. Available from: http://www2.inca.gov.br/wps/wcm/connect/tiposdecancer/site/home/mama. Accessible at: 18 Oct. 2017.

15 CECILIO, A. P. *et al*. Breast cancer in Brazil: epidemiology and treatment challenges. **Breast Cancer:** targets and therapy**,** v. 7, p. 43-49, 2015. DOI: 10.2147/BCTT.S50361.

16 INCA. **Controle do câncer de mama**: tratamento. Available from: http://www2.inca.gov.br/wps/wcm/connect/acoes_programas/site/home/nobrasil/programa_controle_cancer_mama/tratamento . Accessible at: 21 Oct. 2017.

17 BLANCO, K. C.; INADA, N. M.; SALVIO, A. G.; VOLLET FILHO, J. D.; BAGNATO, V. S. Clinical photodynamic therapy review and the brazilian experience. **Journal of Tumor,** v. 4, n. 2, p. 386-392, 2016.

18 CASSIDY, C. M. *et al*. Drug delivery strategies for photodynamic antimicrobial chemotherapy: from benchtop to clinical practice. **Journal of Photochemistry and Photobiology B**: biology**,** v. 95, n. 2, p. 71-80, 2009.

19 DA SILVA, A. P. *et al*. A promising strategy for the treatment of onychomycosis with curcumin and photodynamic therapy. **Journal of Pharmacy and Pharmacology,** v. 3, n. 9, p. 434-437, 2015.

20 ABDEL-KADER, M. H. **Photodynamic therapy**: from theory to application. Berlin: Springer Science & Business Media, 2014.

21 CRUZ-OLIVEIRA, C.; ALMEIDA, A. F.; FREIRE, J. M.; CARUSO, M. B.; MORANDO, M.A.; FERREIRA, V. N. S.; ASSUNÇÃO-MIRANDA, I.; GOMES, A. M. O.; CASTANHO, M. A. R. B.; DA POIAN, A. T. Mechanisms of vesicular stomatitis virus inactivation by protoporphyrin IX, zinc-protoporphyrin IX, and mesoporphyrin IX. **Antimicrobial Agents and Chemotherapy,** v. 61, n. 6, p. 1-14, 2017.

22 ZVEREV, V. V. *et al*. In vitro studies of the antiherpetic effect of photodynamic therapy. **Lasers in Medical Science,** v. 31, n. 5, p. 849-855, 2016.

23 CASTANO, A. P.; DEMIDOVA, T. N.; HAMBLIN, M. R. Mechanisms in photodynamic therapy: part one—photosensitizers, photochemistry and cellular localization. **Photodiagnosis and Photodynamic Therapy,** v. 1, n. 4, p. 279-293, 2004.

24 DENIS, T. G. *et al*. All you need is light: antimicrobial photoinactivation as an evolving and emerging discovery strategy against infectious disease. **Virulence,** v. 2, n. 6, p. 509-520, 2011.

25 BROWN, S. B.; BROWN, E. A.; WALKER, I. The present and future role of photodynamic therapy in cancer treatment. **Lancet Oncology,** v. 5, n. 8, p. 497, 2004.

26 NATIONAL CANCER INSTITUTE. **Photodynamic therapy for cancer**. 2011. Available from: https://www.cancer.gov/about-cancer/treatment/types/surgery/photodynamic-fact-sheet Accessible at: 25 Sept. 2017.

27 AMERICAN CANCER SOCIETY. **Photodynamic therapy**. 2015. Available from: https://www.cancer.org/treatment/treatments-and-side-effects/treatment-types/photodynamic-therapy.html. Accessible at: 29 Sept. 2017.

28 VAN STRATEN, D. *et al*. Oncologic photodynamic therapy: basic principles, current clinical status and future directions. **Cancers,** v. 9, n. 2, p. 19, 2017.

29 AGOSTINIS, P. *et al*. Photodynamic therapy of cancer: an update. **CA**: a cancer journal for clinicians, v. 61, n. 4, p. 250-281, 2011.

30 BAGNATO, V. S. **Terapia fotodinâmica dermatológica**: programa TFD Brasil. São Carlos: Compacta Gráfica e Editora, 2015.

31 BECHET, D. *et al*. Photodynamic therapy of malignant brain tumours: a complementary approach to conventional therapies. **Cancer Treatment Reviews,** v. 40, n. 2, p. 229-241, 2014.

32 ALLISON, R. R.; MOGHISSI, K. Oncologic photodynamic therapy: clinical strategies that modulate mechanisms of action. **Photodiagnosis and Photodynamic Therapy,** v. 10, n. 4, p. 331-341, 2013.

33 CARBINATTO, F. M.; INADA, N. M.; LOMBARDI, W.; DA SILVA, E. V.; BELOTTO, R.; KURACHI, C.; BAGNATO, V. S. Photodynamic therapy of cervical intraepithelial neoplasia (CIN) high grade. **Proceedings of SPIE**, v. 9689, 2016. DOI: 10.1117/12.2213339.

34 GERRITSEN, M. J. P. *et al*. Pretreatment to enhance protoporphyrin IX accumulation in photodynamic therapy. **Dermatology,** v. 218, n. 3, p. 193-202, 2009.

35 ROSSETTI, F. C. *et al*. Optimization of protoporphyrin IX skin delivery for topical photodynamic therapy: nanodispersions of liquid-crystalline phase as nanocarriers. **European Journal of Pharmaceutical Sciences,** v. 83, p. 99-108, 2016. DOI: 10.1016/j.ejps.2015.12.003.

36 DING, H. *et al*. Nanoscopic Micelle delivery improves the photophysical properties and efficacy of photodynamic therapy of protoporphyrin IX. **Journal of Controlled Release:** official journal of the controlled release society**,** v. 151, n. 3, p. 271-277, 2011.

37 SACHAR, M.; ANDERSON, K. E.; MA, X. Protoporphyrin IX: the good, the bad, and the ugly. **Journal of Pharmacology and Experimental Therapeutics**, v. 356, n. 2, p. 267-275, 2016.

38 BRIGGER, I.; DUBERNET, C.; COUVREUR, P. Nanoparticles in cancer therapy and diagnosis. **Advanced Drug Delivery Reviews,** v. 54, n. 5, p. 631-651, 2002.

39 CHEN, C. T. *et al*. Liposome-encapsulated photosensitizers against bacteria. **Recent Patents on Anti-Infective Drug Discovery,** v. 8, n. 2, p. 100-107, 2013.

40 SALAMANCA-BUENTELLO, F. *et al*. Nanotechnology and the developing world. **PLoS Medicine,** v. 2, n. 5, p. e97, 2005.

41 KOO, O. M.; RUBINSTEIN, I.; ONYUKSEL, H. Role of nanotechnology in targeted drug delivery and imaging: a concise review. **Nanomedicine**: nanotechnology, biology and medicine**,** v. 1, n. 3, p. 193-212, 2005.

42 SHI, J. *et al*. Nanotechnology in drug delivery and tissue engineering: from discovery to applications. **Nano Letters,** v. 10, n. 9, p. 3223-3230, 2010.

43 DIMER, F. A. et al. Impactos da nanotecnologia na saúde: produção de medicamentos. **Química Nova,** v. 36, n. 10, p. 1520-1526, 2013.

44 FRÉZARD, F. *et al*. Lipossomas: propriedades físico-químicas e farmacológicas, aplicações na quimioterapia à base de antimônio. **Química Nova,** v. 28, n. 3, p. 511-518, 2005.

45 BATISTA, C. M.; CARVALHO, C. M. B. D.; MAGALHÃES, N. S. S. Lipossomas e suas aplicações terapêuticas: estado da arte. **Revista Brasileira de Ciências Farmacêuticas,** v. 43, n. 2, p. 167-179, 2007.

46 SAFARI, J.; ZARNEGAR, Z. Advanced drug delivery systems: nanotechnology of health design A review. **Journal of Saudi Chemical Society,** v. 18, n. 2, p. 85-99, 2014.

47 CALIXTO, G. M. F. *et al*. Nanotechnology-based drug delivery systems for photodynamic therapy of cancer: a review. **Molecules,** v. 21, n. 3, p. 342, 2016.

48 OHULCHANSKYY, T. Y. *et al*. Organically modified silica nanoparticles with covalently incorporated photosensitizer for photodynamic therapy of cancer. **Nano letters,** v. 7, n. 9, p. 2835-2842, 2007.

49 SHI, J. *et al*. PEGylated fullerene/iron oxide nanocomposites for photodynamic therapy, targeted drug delivery and MR imaging. **Biomaterials,** v. 34, n. 37, p. 9666-9677, 2013.

50 BOVIS, M. J. *et al*. Improved in vivo delivery of m-THPC via pegylated liposomes for use in photodynamic therapy. **Journal of Controlled Release,** v. 157, n. 2, p. 196-205, 2012.

51 RODRIGUEZ, L. *et al*. Aminolevulinic acid dendrimers in photodynamic treatment of cancer and atheromatous disease. **Photochemical & Photobiological Sciences,** v. 14, n. 9, p. 1617-1627, 2015.

52 SUZUKI, I. L. *et al*. Synthesis and characterization of PLGA nanoparticles containing mixture of curcuminoids for optimization of photodynamic inactivation. **Proceedings of SPIE**, v. 9694, 2016. DOI: 10.1117/12.2213781.

53 MURA, S.; NICOLAS, J.; COUVREUR, P. Stimuli-responsive nanocarriers for drug delivery. **Nature materials,** v. 12, n. 11, p. 991-1003, 2013.

54 SINGH, A.; AMIJI, M. M. Stimuli-responsive materials as intelligent drug delivery systems. Available from: https://www.sigmaaldrich.com/technical-documents/articles/materials-science/stimuli-responsive-materials.html. Accessible at: 30 Oct. 2017.

55 KARIMI, M. *et al*. Smart micro/nanoparticles in stimulus-responsive drug/gene delivery systems. **Chemical Society Reviews,** v. 45, n. 5, p. 1457-1501, 2016.

56 VIVERO-ESCOTO, J. L. *et al*. Porphyrin-based polysilsesquioxane nanoparticles to improve photodynamic therapy for cancer treatment. **Proceedings of SPIE,** v. 8931, 2014. DOI: 10.1117/12.2039145.

54 SINGH, A.; AMIJI, M. M. Stimuli-responsive materials as intelligent drug delivery systems. Available from: https://www.sigmaaldrich.com/technical-documents/articles/materials-science/stimuli-responsive-materials.html. Accessible at: 30 Oct. 2017.

55 KARIMI, M. *et al*. Smart micro/nanoparticles in stimulus-responsive drug/gene delivery systems. **Chemical Society Reviews,** v. 45, n. 5, p. 1457-1501, 2016.

56 VIVERO-ESCOTO, J. L. *et al*. Porphyrin-based polysilsesquioxane nanoparticles to improve photodynamic therapy for cancer treatment. **Proceedings of SPIE,** v. 8931, 2014. DOI: 10.1117/12.2039145.

57 BULBAKE, U., DOPPALAPUDI, S., KOMMINENI, N., KHAN W. Liposomal formulations in clinical use: an updated review. **Pharmaceutics**, v. 9, n. 2, p.12, 2017.

58 MANSOORI, M., AGRAWAL, S., JAWADE, S., KHAN, M. A review on liposome. **International Journal of Advanced Research in Pharmaceutical & Biosciences**, v. 2, n. 4, p. 453-464, 2012.

59 SHI, J., KANTOFF, P. W., WOOSTER, R., FAROKHZAD, O. C. Cancer nanomedicine: progress, challenges and opportunities. **Nature Reviews Cancer**, v. 17, n. 1, p. 20-37, 2017.

60 NOMBONA, N., MADURAY, K., ANTUNES, E., KARSTEN, A., NYOKONG, T. Synthesis of phthalocyanine conjugates with gold nanoparticles and liposomes for photodynamic therapy. **Journal of Photochemistry and Photobiology B**: biology, v. 107, p. 35-44, 2012.

61 BUCHHOLZ, J., KASER-HOTZ, B., KHAN, T., BLEY, C. R., MELZER, K., SCHWENDENER, R. A., et al. Optimizing photodynamic therapy: in vivo pharmacokinetics of liposomal meta-(tetrahydroxyphenyl) chlorin in feline squamous cell carcinoma. **Clinical Cancer Research**, v. 11, p. 7538-7544, 2005.

62 KIM, J., SANTOS, O. A., PARK, J-H. Selective photosensitizer delivery into plasma membrane for effective photodynamic therapy. **Journal of controlled release**, v. 191, p. 98-104, 2014.

63 HAMBLIN, M. R.; DEMIDOVA, T. N. Mechanisms of low level light therapy. **Proceedings of SPIE,** v. 6140, 2006. DOI: 10.1117/12.646294.

64 SIGMA-ALDRICH. **Product information**: MTT. Available from: https://www.sigmaaldrich.com/content/dam/sigma-aldrich/docs/Sigma/Usage/m5655use.pdf. Accessible at: 30 Oct. 2019.

65 KELBAUSKAS, L.; DIETEL, W. Internalization of aggregated photosensitizers by tumor cells: subcellular time-resolved fluorescence spectroscopy on derivatives of pyropheophorbide-a ethers and chlorin e6 under femtosecond one-and two-photon excitation. **Photochemistry and Photobiology,** v. 76, n. 6, p. 686-694, 2002.

66 KRESS, M.; MEIER, T.; STEINER, R.; DOLP, F.; ERDMANN, R.; ORTMANN, U.; RU, A. Time-resolved microspectrofluorometry and fluorescence lifetime imaging of photosensitizers using picosecond pulsed diode lasers in laser scanning microscopes. **Journal of Biomedical Optics**, v. 8, n. 1, p. 26-32, 2003.